TECHNICAL REPORT ECOM-00212-F

STUDY OF EFFECT OF HIGH-INTENSITY PULSED NUCLEAR RADIATION ON ELECTRONIC PARTS AND MATERIALS (SCORRE)

FINAL REPORT

BY
P.G. BOCZAR - G.E. BOYD
W.A. CORDWELL - F.A. FRANKOVSKY

OCTOBER 1966

ECOM

UNITED STATES ARMY ELECTRONICS COMMAND-FORT MONMOUTH, N.J.

CONTRACT DA28-043-AMC-00212(E)
IBM ELECTRONICS SYSTEMS CENTER, Owego, N.Y.

"This research is sponsored by the Defense Atomic Support Agency under NWER Subtask 16.0091."

Distribution of this document is unlimited.

Disclaimers

The findings in this report are not to be construed as an official Department of the Army position, unless so designated by other authorized documents.

The citation of trade names and names of manufacturers in this report is not to be construed as official Government indorsement or approval of commercial products or services referenced herein.

Disposition

Destroy this report when it is no longer needed. Do not return it to the originator.

TECHNICAL REPORT ECOM-00212-F OCTOBER 1966

STUDY OF EFFECT OF HIGH-INTENSITY PULSED NUCLEAR RADIATION ON ELECTRONIC PARTS AND MATERIALS (SCORRE)

FINAL REPORT

15 JUNE 1964 TO 15 JULY 1966

Report No. 6

CONTRACT DA28-043-AMC-00212(E)

DA Project No. 5901.21.700.01

Prepared By

PAUL G. BOCZAR GILBERT E. BOYD

WAYNE A. CORDWELL FRANK A. FRANKOVSKY

IBM ELECTRONICS SYSTEMS CENTER, OWEGO, N.Y.

For

UNITED STATES ARMY ELECTRONICS COMMAND, FORT MONMOUTH, N.J.

This research is sponsored by the Defense Atomic Support Agency under NWER Subtask 16.009.

ABSTRACT

This report describes the radiation-induced behavior of tantalum-oxide, mica, ceramic, Mylar, glass, and polystyrene capacitors using results obtained at several sources. Also included are discussions of the following:

- Experimental techniques at each radiation source, including measurement of circuits, components, dosimetry, and variation of circuit and radiation parameters;
- Results from SPRF, LINAC, and AFXR tests describing the dependences of the induced current for the irradiated dielectric;
- Interpretation of these results in terms of appropriate models and radiation and circuit parameters;
- Comparison of the effects observed at each irradiation source;
- Description of the tests on magnetics and the test results.

TABLE OF CONTENTS

Table of Contents (cont)

Table of Contents (cont)

LIST OF ILLUSTRATIONS

LIST OF TABLES

Section I

INTRODUCTION

The primary objective of transient radiation effects studies in electronic parts and materials is to determine radiation hardness design information over a wide range of radiation levels. Circuit design demands intensive radiation effects studies on dielectric and magnetic devices utilizing sources emitting gamma rays, electrons, neutrons, and X-rays at various energies and with various pulse durations.

Under contract to ECOM, IBM has investigated the effects of nuclear radiation pulses on dielectric and magnetic devices. Numerous experiments have been performed at a variety of pulsed radiation sources, including pulsed reactors, linear accelerators, and advanced flash X-ray machines. These tests on dielectric devices have resulted in the formulation of a theoretical model to explain the radiation-induced conductivity in dielectrics, and have yielded sufficient experimental data to supply many of the parameters to be used in this model.

The purpose of the magnetics tests was to collect data on the operation of several selected magnetic devices at high gamma dose rates, such as those generated in the prompt portion of a weapon burst. This data will be used to determine if more extensive testing of a variety of magnetic materials should be performed. Testing has shown no effects which will cause malfunction of these magnetic devices when used for data storage at dose rates in excess of 10^{11} rad/s.

During the past 2 years, extensive tests were performed to compare the currents induced in several commercial capacitors by nuclear radiation from a pulsed reactor (SPRF), with those induced by the electron beam of a linear accelerator (LINAC). Analysis of the LINAC data has given further information for the characteristic amplitude parameters, K_p and K_{dn}, and the delay time constants, τ_{dn}. These results indicate that the radiation-induced conductivity effects are consistent with data obtained in the pulsed-reactor environment. This consistency was obtained only after consideration of the relative effectiveness of neutron and gamma radiation in producing currents in the capacitive elements at the reactor environment (Reference 1).

To confirm the capability of the electron band model to predict behavior for the combination of high dose rates and short pulse widths, experiments were also performed at an Advanced Flash X-Ray (AFXR) source. This source provides dose rates on the order of 10^{11} rad/s, with pulse widths

ranging from about 30 to 100 ns. Presently, only the behavior of tantalum oxide has been analyzed at this source. Results indicate the band model is applicable to a combination of high dose rates and short pulse widths, and that radiation-induced currents vary linearly with dose rate, capacitance, and applied voltage at high dose rates. No effects resulting in a loss of information in magnetic elements were produced by AFXR irradiation at dose rates as high as 2×10^{11} rad/s.

Temperature effects on carrier mobility and lifetime were also studied in tantalum-oxide and ceramic dielectrics. With a simple band model having a single electron trapping level a few kT below the conduction band (E_{nT}), tantalum-oxide yields a trapping level of about 0.2 eV at both LINAC and AFXR (Reference 2).

Section II

DIELECTRIC PROGRAM

A. SUMMARY OF THE DIELECTRIC PROGRAM

Table 1 lists the capacitor types that have been studied under the present contract and the present understanding of their behavior at various types of sources. The "theory" column indicates dielectrics for which experimental results to date are understood in terms of physical mechanisms, and which have a model and relationships to describe the required dependences.

Table 1

DIELECTRIC PROGRAM

Capacitor Type	SPRF		LINAC	AFXR	Theory
	Gamma	Neutron			
Mica	●	Q	●	X	●
Tantalum Oxide	●	Q	●	O	●
Glass	Q	X	O	X	Q
Ceramic	Q	X	O	O	Q
Mylar	●	Q	●	X	●
Polystyrene	●	Q	●	X	●

Legend:

● Considered complete in capacitor characterization
O Partially completed
Q Results to date are questionable
X No work done as yet

B. THEORETICAL CONSIDERATIONS

The general relationship for the conductivity of a capacitor under irradiation (Reference 3) has been shown to be

$$\frac{\sigma - \sigma_o}{\epsilon \epsilon_o} = K_p \dot{D}(t) + \sum_n K_{d_n} \int_{-\infty}^{t} e^{-(t-t')/\tau_{d_n}} \dot{D}(t')dt', \qquad (1)$$

which is related to the radiation-induced current by the equation

$$i_r = \frac{(\sigma - \sigma_o)}{\epsilon \epsilon_o} CV.$$

This gives

$$i_r = CV\left[K_p \dot{D}(t) + \sum_n K_{d_n} \int_{-\infty}^{t} e^{-(t-t')/\tau_{d_n}} \dot{D}(t')\, dt',\right] \qquad (2)$$

where

σ_o = the dark conductivity in the absence of radiation

ϵ = the dielectric constant

ϵ_o = permittivity of free space

K_p and K_d = empirically determined parameters for the radiation-induced conductivity effect

τ_{d_n} = time constants

$\dot{D}(t)$ = the radiation exposure rate

i_r = the radiation induced current.

When the radiation field contains several mixed components of radiation, $\dot{D}(t)$ must contain a contribution from each environment. The total field can

be written as a linear combination of the components. The total effect, $\dot{D}(t)$, at a pulse reactor can be written as the linear sum of a neutron and gamma field:

$$\dot{D}(t) = F\dot{N}(t) + \dot{\gamma}(t), \tag{3}$$

where

F = proportionality constant relating the absorbed dose rate from the neutron spectrum to an equivalent absorbed gamma dose rate

$\dot{N}(t)$ = equivalent absorbed gamma dose rate.

If one defines a ratio $R = \dot{N}(t) / \dot{\gamma}(t)$, then

$$\dot{D}(t) = \left[FR + 1 \right] \dot{\gamma}(t). \tag{4}$$

The radiation-induced current is then given by

$$i_r(t) = CV\left[K_p \dot{\gamma}(t)(FR+1) + \sum_n K_{d_n} \int_{-\infty}^{t} e^{-(t-t')/\tau_{d_n}} (FR+1)\, \dot{\gamma} dt' \right] \tag{5}$$

Several analytical techniques have been developed for solving Equation (5) and are documented in Reference 1, which also describes empirical conditions to determine the characteristic parameter F relating the two fields.

At a pulsed electron source, such as LINAC, having a square radiation pulse with amplitude D(t) and duration t_p, the radiation-induced current can be expressed as a kernel in time over the two domains of interest, $t \leq t_p$ and $t \geq t_p$. Equation (2) then reduces to

$$i_r(t) = \begin{cases} CV\left[K_p \dot{D}(t) + \sum_n K_{d_n} \tau_{d_n} \dot{D}(1 - e^{-t/\tau_{d_n}}) \right], & \text{for } t \leq t_p \\ CV\, \dot{D}(t) \sum_n K_{d_n} \tau_{d_n} (e^{t_p/\tau_{d_n}} - 1) e^{-t/\tau_{d_n}}, & \text{for } t \geq t_p \end{cases} \tag{6}$$

Applying Equation (6) to the dielectric responses observed at a LINAC, K_p and the first delay components, $K_{d_1} \tau_{d_1}$, can usually be determined.

However, later components (K_{d_n} τ_{d_n},) are difficult to determine accurately from this measurement. To obtain further information on these later components, the total charge replenished to the capacitor is measured and an expression relating the replenished charge to these parameters is derived. This expression is given by

$$Q_T = CV\dot{D}t_p \left[K_p + \sum_n K_{d_n} \left(\tau_{d_n} - \frac{t_p}{2} \right) \right] . \tag{7}$$

When the pulse width, t_p, is much smaller than τ_{d_n}, Equation (7) can be approximated by

$$Q_T \sim CV\dot{D}t_p \left[K_p + \sum_n K_{d_n} \tau_{d_n} \right] . \tag{8}$$

Equations (6) and (7) can be used to determine the parameters necessary to characterize a given dielectric material in a transient radiation environment, except for the parameter F, which is obtained from the neutron environment.

C. CIRCUITS USED TO MEASURE DIELECTRIC RESPONSES

The transient conductivity of a capacitor is determined from the measurement of the radiation-induced current. A supplementary measurement is the replenished charge, which is the integral of the radiation-induced current in either lead, and is obtained manually (from the picture of the current display) or electronically (by integrating the current signal).

Two methods were used to monitor the radiation-induced current transients:

- Measuring the voltage drop across a sampling resistor in series with the capacitive element
- Measuring the output of a current transformer (current probe) in series with the exposed capacitor.

1. RESISTOR SAMPLING

Figure 1 is the circuit used for measuring radiation-induced current by the resistor method. This circuit was used when maximum sensitivity was required or when the time duration of the transient current exceeded the pulse width capability of current probes. The circuit components are defined by the following:

- Z_0 is equal to the cable characteristic impedance.
- C is the power supply cable bypass capacitance. It is large enough to provide a stiff voltage source during the radiation transient.
- R1 is selected to satisfy one of the conditions:
  a. For best pulse response, set R1 equal to Z_0
  b. For maximum sensitivity, R1 may be omitted
  c. When sensitivity is not critical, and operating point deviations are held to a minimum, keep R1 very small.
- R2 must isolate the power supply from the measurement circuit during the transient and is much larger than R1 and Z_0 in parallel.

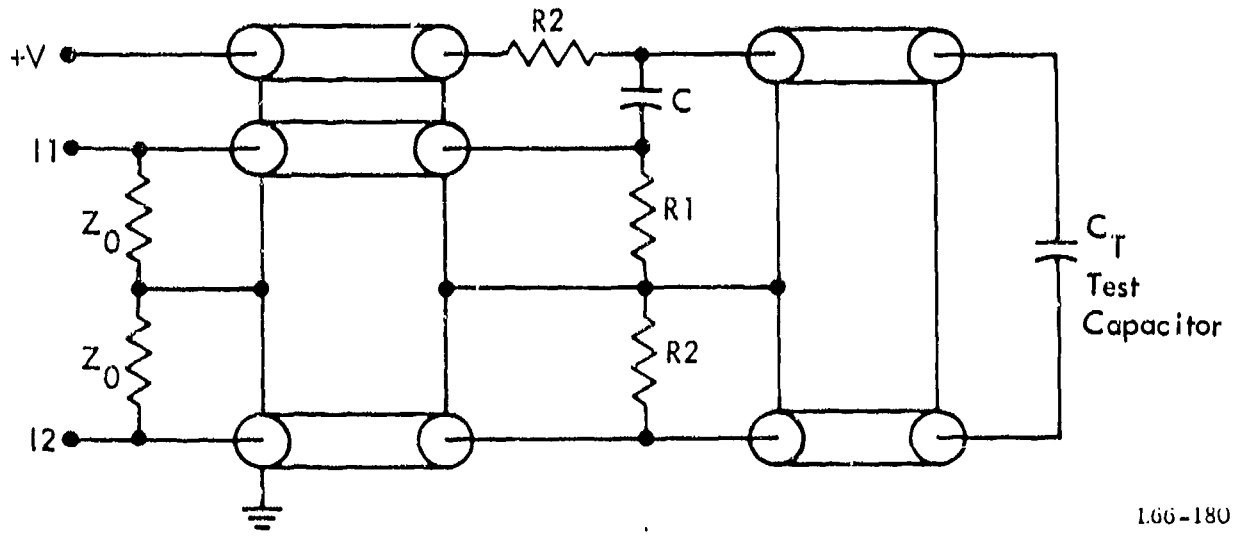

Figure 1. Circuit for Measuring Induced Current (Resistor Method)

2. CURRENT PROBE SAMPLING

Figure 2 is the measuring circuit for radiation-induced currents, using the current probe method. The circuit components are defined as follows:

- Z_0 is equal to the cable characteristic impedance
- C is the power supply cable bypass capacitance. It is sufficiently large to provide a stiff voltage source during the radiation transient.
- CT-2 is a current transformer with suitable response. When the integrating circuit is used to measure the total replenished charge ($Z_1 Z_f$), the time constant of the integrator must be very long when compared with the period of integration to have a negligible loss of charge.

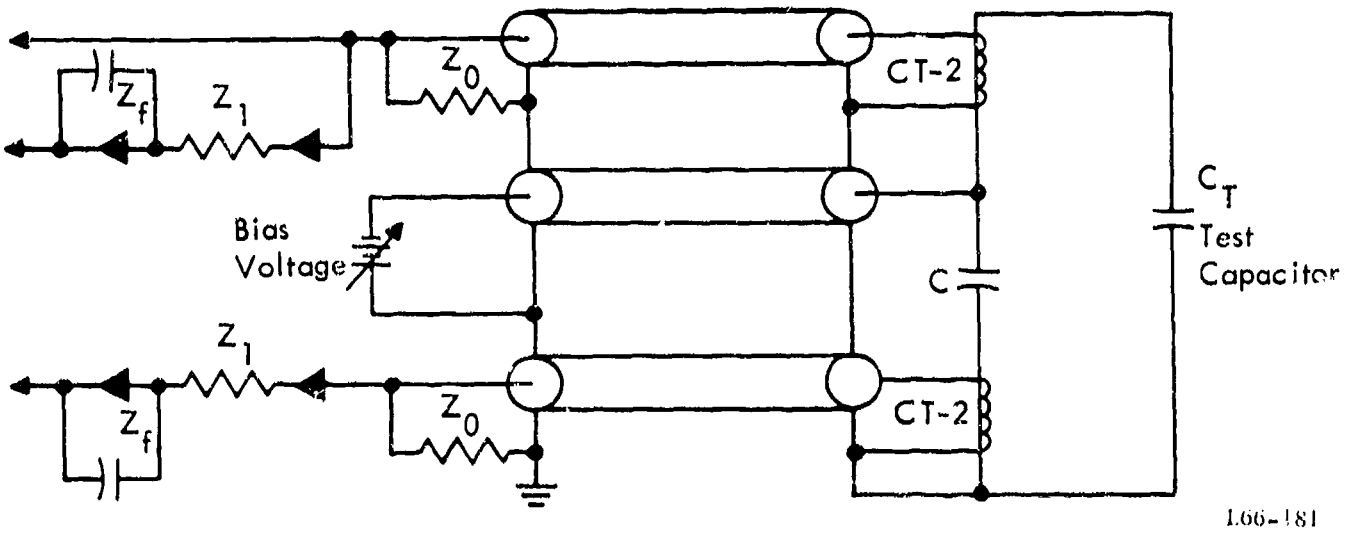

Figure 2. Circuit for Measuring Induced Current (Current Probe Method)

D. DIELECTRIC CHARACTERIZATION

1. PULSED REACTOR (SPRF) TEST

a. Reactor Description

The Sandia Pulsed Reactor (SPRF) is a bare critical assembly having a pulse width of 50 μs at half-maximum. The average neutron energy is 1.4 MeV and the average gamma energy is 0.8 MeV. Nominally, at 9-1/4 inches, the gamma dose rate is 4.5×10^6 rad/s and the neutron flux is 6×10^{16} n/cm^2-s (E >10 keV). The flux has a $1/r^2$ fall-off (Reference 4 and 5). Polyethylene and lead shields were used to vary the neutron-to-gamma ratio over a factor of eight.

b. Test Description

Six different dielectric types were studied at the pulsed reactor with the measuring circuit shown in Figure 1. Wide variations in the insulating layer thickness capacitance, surface area, and insulator volume were chosen for each dielectric type. Voltages were applied in the direction of high resistivity and covered the range from zero to the rated voltage (WVdc). To reduce currents through air ionization paths, the capacitors and exposed ends of the transmission cables were potted with a Silastic* compound.

Experiments were conducted to obtain data on the radiation-induced current as a function of:

- Alteration of the neutron-to-gamma-ray ratio ($\dot{N}/\dot{D}$), with variations of dose and dose rate
- Variations of capacitance, applied voltage, and d-c working voltage (WVdc).

c. Reactor Test Results

The reactor-induced dielectric characterization (Reference 1) is summarized in Table 2.

2. ELECTRON LINEAR ACCELERATOR

a. Source Description

Two sources were used for this work. The General Atomic Electron Linear Accelerator (LINAC) was used to deliver single pulses of electrons having an energy of about 18 MeV. The pulse widths were varied from 0.3 to 4.5 μs with a peak current near 200 mA. The maximum dose rates achieved for ± 5-percent uniformity on sample irradiation were about 1×10^{10} rad/s.

The White Sands LINAC was also used at an electron energy between 10 to 12 MeV. Pulse widths were varied from 0.1 to 2.0 μs with a peak beam current near 450 mA. The maximum dose rates achieved for ± 5-percent uniformity of sample irradiation were approximately 10^9 rad/s.

b. Test Description

The primary purpose of the LINAC test series was to further characterize the dielectric response of capacitors and to compare the differences between reactor- and electron-accelerator- induced conductivities. Six different

---

* Registered trademark of Dow Corning Corporation.

Table 2

PULSED-REACTOR TABULATION OF PARAMETERS

Dielectric	K_p (10^{-6} rad^{-1})	K_{d_2} (10^{-2} $(rad\text{-}s)^{-1}$)	τ_{d_2} (10^{-3} s)	F* (rad-cm^2/n)	i_n/i_T**
Tantalum Oxide	9	4.5	1	6.5×10^{-11}	0.24
Ceramic	±1	---	---	---	---
Mica	4	none	none	1.4×10^{-11}	0.06
Mylar	12	---	---	3.2×10^{-10}	0.60
Polystyrene	14	4.7	1	1.3×10^{-9}	0.80
Glass	10	---	---	---	---

* F is a proportionality constant relating the absorbed dose rate due to fission neutrons to an equivalent absorbed gamma dose rate. All gamma energy loss is considered due to ionization.

** i_n/i_T, the relative neutron effectiveness due to a mixed field, pertains only to the prompt portion of the radiation. Induced current is derived from the fission spectrum for exposures at SPRF. This ratio is given for a normal burst with a specific $\dot{N}/\dot{D}$ value of 3.3×10^9 n/cm^2 /rad.

dielectric materials, covering a complete range in capacitor geometry, were exposed to varying LINAC parameters of beam current, electron energy, dose, dose rate, and pulse width.

Mylar, polystyrene, mica, glass, tantalum-oxide, and ceramic capacitors were tested at several different voltages, capacitances, and working voltages (WVdc). In addition, tantalum-oxide and ceramic capacitors were exposed in a controlled temperature environment in a commercially converted oven over a range of 0°C to 85°C. Temperature was controlled by cycling between electronic heaters and a liquid carbon dioxide coolant. A blower maintained the oven chamber at any set temperature ±1°C (Reference 6).

Current probes were used to monitor the induced current through both leads of the capacitor. An integrating circuit measured the total replenishment charge through each capacitor lead. The second probe was used as an

aid for separating radiation-induced emission in the wiring and sample configuration from a true dielectric response.

The actual testing was performed inside an aluminum box to shield the experiment from radio-frequency (R-F) interference. No special encapsulations or pottings were used on the capacitor elements tested, since the magnitude of charge scattering effects could be inferred from the measurements. Coaxial transmission lines were covered with shielded zipper tubing to reduce R-F interference. Radiation effects were eliminated on the components required in the measuring circuit and on cable ends, by housing the circuit inside an aluminum and lead shield containing feed-through connections to the test sample.

c. LINAC Results

Data tables including pulse widths, dose rates, applied voltages, and currents observed for each dielectric tested at LINAC are presented in detail in References 1 and 2. Reference 2 also lists the estimates of the long delay time constant (τ_{d_2}) for Mylar and polystyrene as obtained from measuring the total replenishment charge. Table 3 presents a summary of this LINAC work, and Table 4 compares the parameters observed at LINAC and at SPRF. Where the delay constants (τ_d) are short, the observation ($K_p + K_d \tau_d$) at LINAC is compared to the neutron-corrected K_p value observed at SPRF. The small τ_d values resolved in the LINAC work are not seen at SPRF but are included in its prompt response due to the longer time domain of the excitation pulse. Table 4 shows very good agreement between the SPRF and LINAC results with the largest discrepancy about a factor of three observed for ceramic. Of the six dielectrics tested, tantalum oxide has been the most extensively studied and characterized. At LINAC dose rates ranging between, 10^8 and 10^{10} rad/s, tantalum oxide has the smallest K_p value and shortest delay constant of the tested dielectrics. Several physical parameters inherent in the tantalum-oxide material have also been estimated at these dose rates. These include an electron mobility of approximately 10^{-5} cm^2 $(volt\text{-}s)^{-1}$ and a generation rate of 4.6×10^{12} pairs $(rad\text{-}cm^3)^{-1}$, corresponding to about 136 eV to create an electron hold pair (Reference 1).

3. ADVANCED FLASH X-RAY

a. Source Description

Advanced Flash X-Ray testing was performed at the Physics International energy facility which has a 5-million volt peak energy source. Figure 3 shows the location of the instrument room, irradiation room, and pulser controls.

Table 3

LINAC* TEST RESULTS

Dielectric	K_p (rad^{-1})	K_{d_1} (10^{-2}(rad-s)$^{-1}$)	τ_{d_1} (μs)	K_{d_2} (10^{-2}(rad-s)$^{-1}$)	τ_{d_2} (μs)
Tantalum Oxide	5×10^{-7}	4.2	0.85	3.6	200
Ceramic	$\pm 3.2 \times 10^{-7}$	---	---	---	---
Mica	4.2×10^{-6}	none	none	none	none
Mylar	2.5×10^{-6}	0.24	8	1	500
Polystyrene	3.0×10^{-6}	0.07	10	4	300
Glass	1.5×10^{-5}	---	---	---	---

* General Atomic and White Sands as sources

Table 4

DIELECTRIC PARAMETERS COMPARED

Dielectric	LINAC (rad/s)	SPRF (10^{-6} rad/s)
Tantalum Oxide	3.6×10^{-6} ($K_p + K_{d_1} \tau_{d_1}$)	*6.8
Ceramic	$+3.2 \times 10^{-7}$ (K_p)	±1.0
Mica	4.2×10^{-6} (K_p)	*3.7
Mylar	4.48×10^{-6} ($K_p + K_{d_1} \tau_{d_1}$)	*4.8
Polystyrene	3.0×10^{-6} (K_p)	*2.7
Glass	1.5×10^{-5} (K_p)	10

* K_p values are neutron corrected.

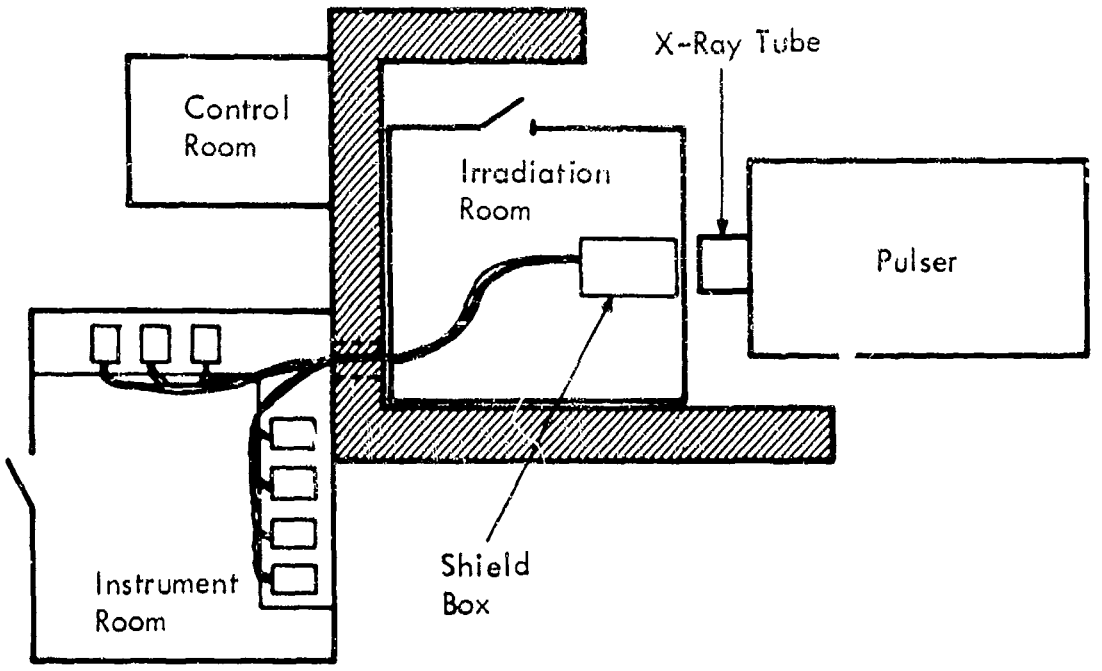

Figure 3. Physics International Energy Facility (Diagram)

b. Test Description

The instrumentation and irradiation rooms are both double shielded rooms. Because the noise level in the irradiation room is too high to allow sensitive measurements, an aluminum shield box was used to reduce the noise to an acceptable level. Signal transmission lines were triaxial RG58A cables enclosed in aluminum zipper tubing. Figure 4 shows the sample location inside the shield box and the lead shield used to protect the current probes and cable connectors from the X-ray beam.

A lead shield, approximately 6 inches thick, was used to obtain a dose reduction at the current-probe box to less than 1 percent. Oscilloscopes were triggered by one photodiode and the output of a second was recorded to provide burst shape information. Two capacitor samples were irradiated simultaneously and the currents in each lead were monitored. The integral of the current in one lead of each component was measured with a Type-0 Tektronix operational amplifier and recorded on oscilloscopes. Data were recorded by photographing the displays of seven Type-647 Tektronix oscilloscopes with solenoid-operated shutters.

Both ceramic and tantalum-oxide dielectrics have been irradiated at AFXR. Radiation-induced effects were determined for both dielectrics as a

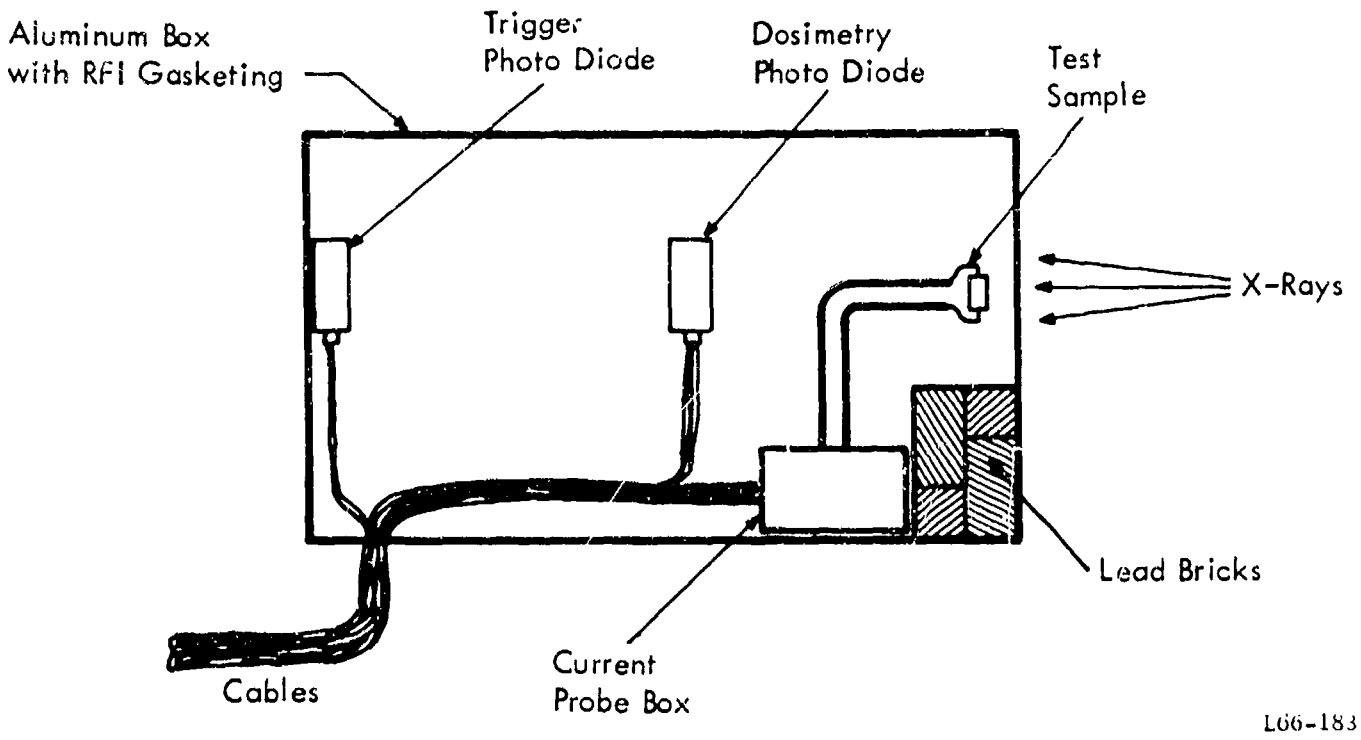

Figure 4. Aluminum Shield Box

function of voltage, temperature, and capacitance value. A dose rate dependence test was performed for tantalum-oxide.

c. AFXR Test Results

The data for the dielectrics tested at the AFXR are presented in Tables 5 through 9. Those entries marked with an asterisk represent oscillograph pictures that could not be used due to improper scale factor settings, noise distortion, or camera failure.

(1) Tantalum-Oxide Capacitors

Table 5 shows the results of the maximum current observed for dose rate variation in a tantalum-oxide capacitor, with temperature, applied voltage, and capacitance remaining constant. The dose rate was varied from 2.51×10^{9} to 1.81×10^{11} rad/s.

Figure 5 shows the plot of the data in Table 5. The results show that the maximum induced-current varies linearly with dose rate at these high levels; i. e., the power of delta to which the dose rate is raised is one, showing that saturation effects do not occur.

Table 5

DOSE RATE VARIATIONS FOR A 1- μF TANTALUM-OXIDE CAPACITOR

Pulse Number	V_A (volts)	I_1 (mA)	I_2 (mA)	t_p (μ s)	Burst $\dot{D}$ (rad/s)
336	90	800	800	0.1	1.81×10^{11}
331	90	440	440	0.1	1.00×10^{11}
332	90	390	390	0.1	8.16×10^{10}
333	90	82	82	0.1	1.91×10^{10}
334	90	16	16	0.1	3.32×10^{9}
335	90	13.5	13.5	0.1	2.51×10^{9}

Measurements taken with temperature, capacitance, and applied voltage constant

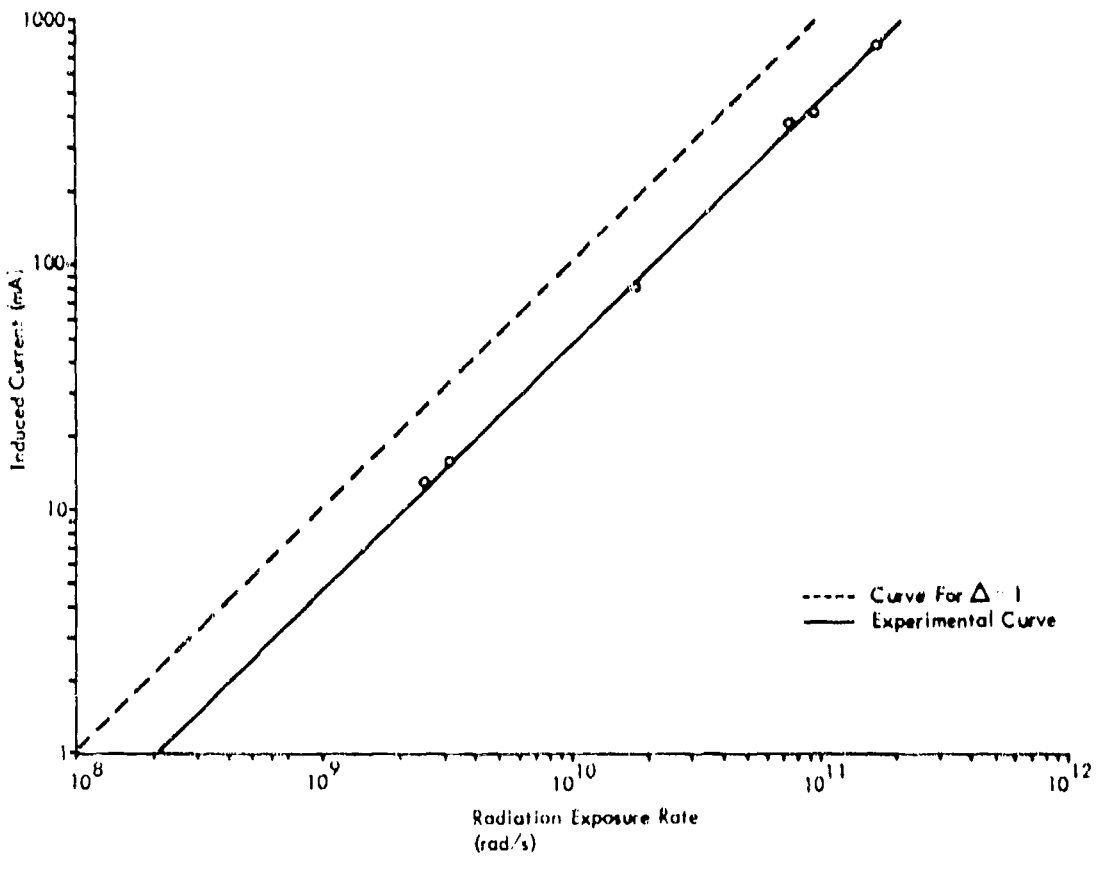

L66-184

Figure 5. Induced Current Versus Dose Rate Variations for a 1- μF Tantalum-Oxide Capacitor

The temperature data in Table 6 is shown in Figure 6 as the maximum current per CVD versus temperature. The increase of current with temperature is exponential over the range from 0°C to 85°C. These results give a trapping level of 0.15 eV and are comparable to the LINAC work shown later in this report. The temperature variations are discussed later in detail.

Table 6

TEMPERATURE VARIATIONS FOR A 1-μF 100-WVdc TANTALUM-OXIDE CAPACITOR (SAMPLE 42)**

Variations			Ground Side i_2	Voltage Side i_1	Voltage Side (10^{-6} coulombs)	Burst $\dot{D}$ (10^{10} rad/s)	
Pulse	Temperature (C°)	V_A (volts)	m_A	m_A	Q_{T_1}	Minimum	Maximum
1	20	79.7	259.7	*	*	5.87	7.33
2	20	79.7	425.9	427	3.81	7.07	7.07
3	40	79.7	561	545	4.64	6.68	7.84
4	50	79.7	768	763.6	6.0	8.26	9.51
5	60	79.7	779	790	5.64	6.27	7.99
6	85	79.7	1221	1227	7.64	7.44	8.05

* Missing data point
** At constant capacitance, applied voltage, and near-constant dose rate

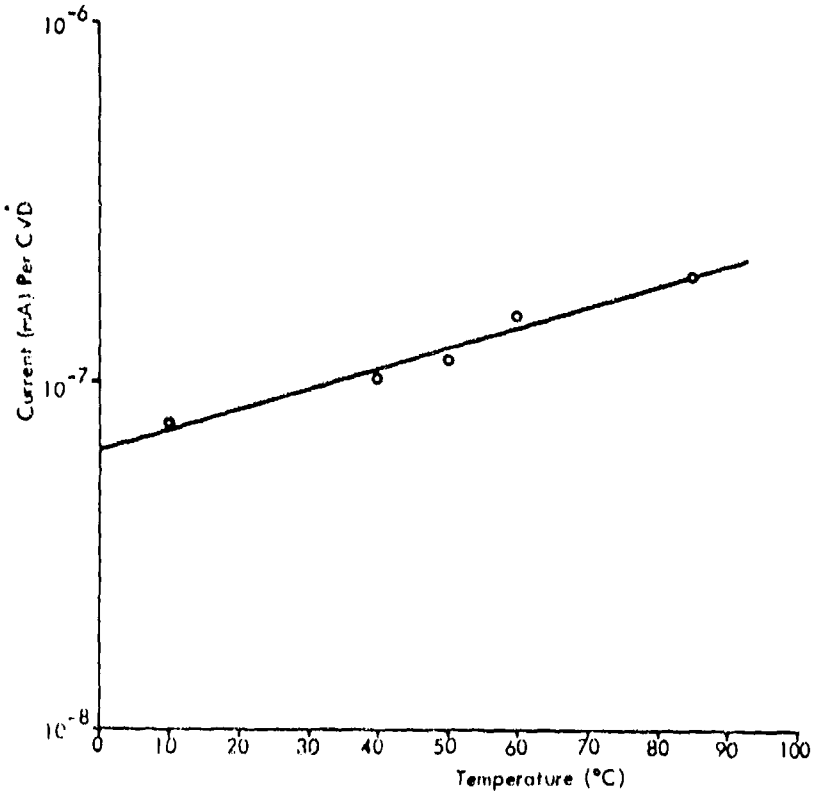

I.66-185

Figure 6. Current per CVD Versus Temperature for a 1-μF 100-WVdc Tantalum-Oxide Capacitor

Table 7 presents the data, and Figure 7 shows the plot of radiation-induced current versus time for several different applied voltages. After reaching their maximum value, the curves fall in a straight line, indicating that the decay is exponential and can be considered due to one time delay constant over this time domain. Analytical techniques have been developed to fit these responses to the curve. The results will appear in the next quarterly report.

Table 7

VOLTAGE VARIATIONS FOR TANTALUM-OXIDE CAPACITORS (SAMPLES 42 AND 45)**

Variations		Ground Side i_2 (mA)	Voltage Side i_1 (mA)	Voltage Side (coulombs) Q_{T_1}	Burst Variations $\dot{D}$ (10^{11} rad/s)	
Pulse	V_A (volts)				Minimum	Maximum
SAMPLE 42 — 1 μF, 100 WVdc						
1	0	14.54	9.63	*	1.28	1.38
2	20	145	140	*	1.06	1.2
3	40	*	343	2.68×10^{-6}	1.25	1.41
4	70.7	623	626	5.3×10^{-6}	1.24	1.25
5	94.2	909	915.7	*	1.26	1.28
SAMPLE 45 — 47 μ F, 100 WVdc						
1	5	259.7	254	*	1.07	1.44
2	10	540	527	*	1.15	1.62
3	15	701	704	*	1.31	1.51
4	20	1039	1000	3.6×10^{-5}	1.0	1.29
5	30	2590	2727	9.1×10^{-5}	1.26	1.68

* Missing data point
** At constant temperature, and near-constant dose rate

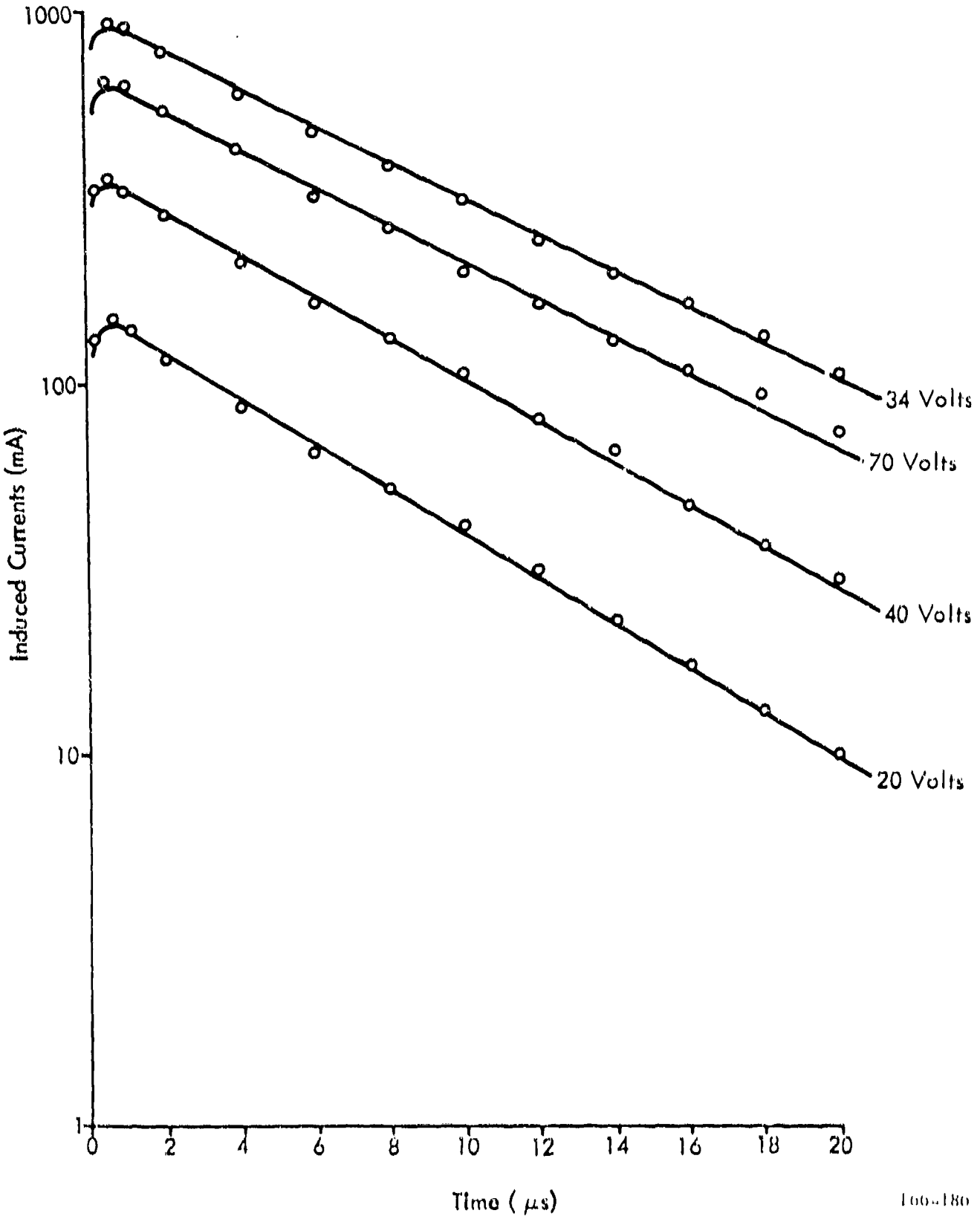

Figure 7. Voltage Variations for a 1- μF 100-WVdc Tantalum-Oxide Capacitor (Sample 42)

(2) Ceramic Capacitors

Tables 8 and 9 present the data obtained for ceramic capacitors irradiated at AFXR. Table 8 lists the voltage dependences data and Table 9 indicates the effects of temperature variation at constant applied voltage. Figure 8 shows the temperature effects on capacitance.

Table 8

VOLTAGE VARIATIONS FOR CERAMIC CAPACITORS (SAMPLES 54 AND 55)

Variations		Ground Side	Voltage Side	Burst $\dot{D}$ (10^{11} rad/s)	
Pulse	V_A(volts)	i_2 (mA)	i_1 (mA)	Minimum	Maximum
SAMPLE 54– 0.1 μF					
1	0	3.1	4.3	1.4	1.47
2	10	9.35	9.64	1.14	1.29
3	20	3.31	8.67	1.169	1.25
4	30	22.34	22.16	2.0	2.13
5	40	18.7	19.3	1.37	1.4
6	45	16.62	19.3	1.728	1.728
SAMPLE 55 – 1 μF					
1	0	0.75	7.73	1.079	1.15
2	5	18.7	20.0	1.4	1.44
3	10	21.8	21.8	1.1	1.18
4	15	39.48	40	1.64	1.72
5	20	32.2	31.8	1.217	1.32
6	24	47.79	49.2	1.75	1.83

Table 9

TEMPERATURE VARIATIONS FOR A 0.1- μF
50-WVDC CERAMIC CAPACITOR (SAMPLE 53)

Variations			Ground Side i_2(mA)	Voltage Side i_1(mA)	Capacitance (μF)	Burst D (10^{10} rad/s)	
Pulse	Temperature (°C)	V_A(volts)				Minimum	Maximum
1							
2	20	10	0.56	0.56	0.0933	8.59	9.98
3	40	10	0.26	0.24	0.0937	8.82	8.94
4	50	10	----	0.28	0.0870	10.14	10.7
5	60	10	----	0.15	0.0780	8.97	9.83
6	85	10	0.07	0.08	0.0495	9.37	9.49

4. METHODS OF CURVE-FITTING DIELECTRIC PARAMETERS

Since the radiation-induced currents in dielectrics have the dose rate as their driving function, the burst shape must be processed to achieve a current source usable in a circuit analysis program. Transient Radiation Effect Automated Tabulation (TREAT) was the processing method used for this data (Reference 7). Figure 9 illustrates the flow of the data processing steps.

The disadvantage of the technique is that changes in the weapon profile or radiation model parameters require recomputation of radiation current sources by TREAT, and of radiation transient response by the transient circuit analysis program. The recomputation of radiation transient response is unavoidable. However, a method of feeding the burst shape and radiation model parameters directly into the transient circuit analysis program could save considerable time.

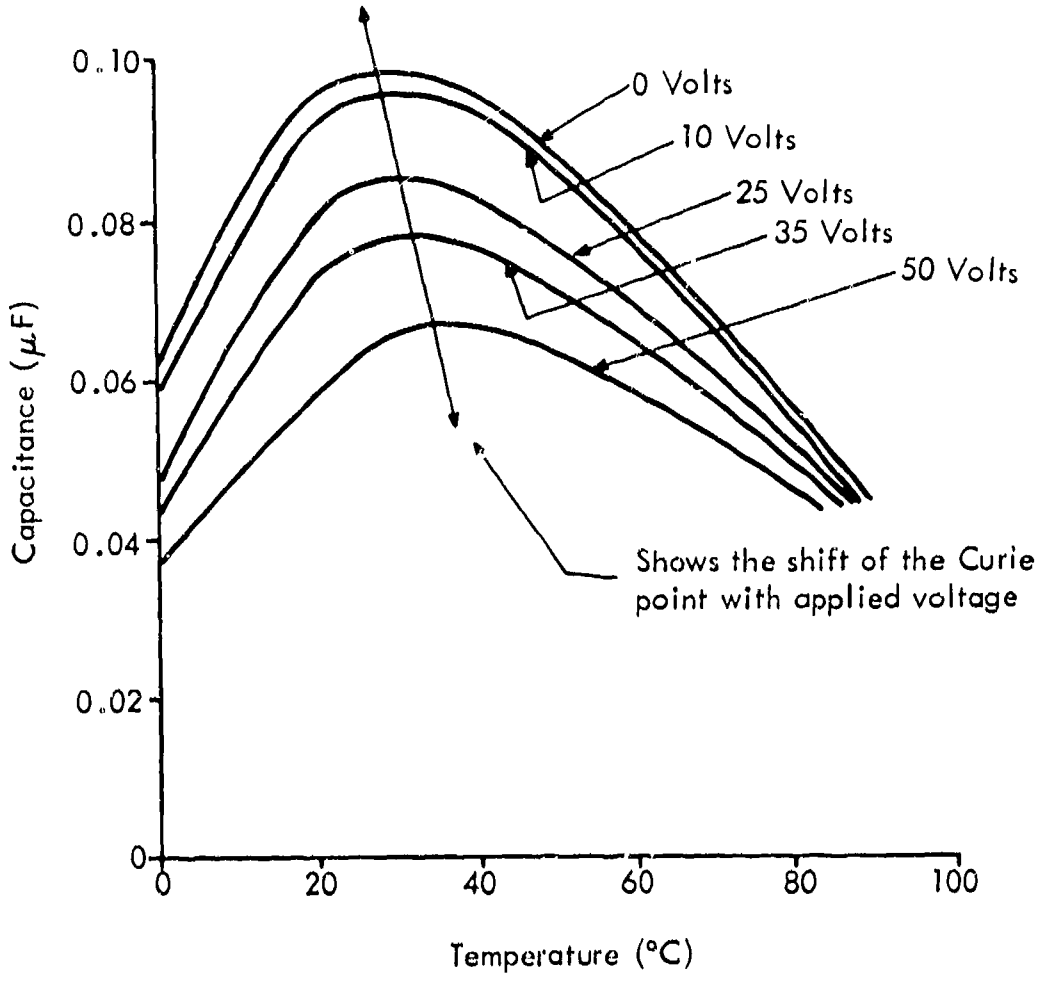

L66-187

Figure 8. Effect of Temperature on a 0.1- μF 50-WVdc Ceramic Capacitor (Sample 53)

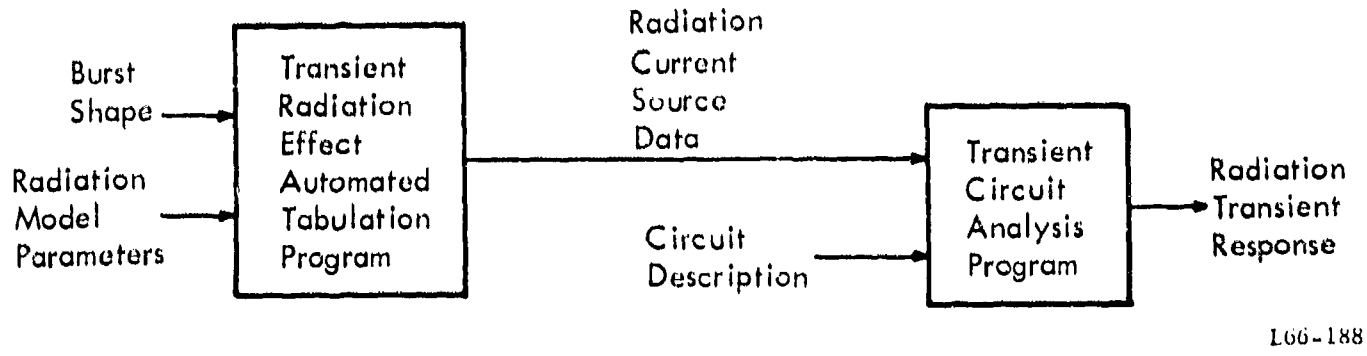

L66-188

Figure 9. Curve-Fitting Dielectric Parameters to Experimental Results

Two direct methods for determining radiation-induced transient currents by a transient circuit analysis program are discussed below:

a. Convolution

The response of a network can be expressed as

$$e_{out}(t) = \int_o^t e_{in}(\lambda)\, h(t-\lambda)\, d\lambda, \tag{9}$$

where

$e_{out}(t)$ = output voltage

$e_{in}(t)$ = the input voltage

$h(t)$ = the network response to an impulse function.

The R-C network shown in Figure 10 has an impulse response $h(t) = 1/RC\ e^{-t/RC}$. Therefore,

$$e_{out}(t) = \frac{1}{RC}\int_o^t e_{in}(\lambda)\, e^{-(t-\lambda)/RC}\, d\lambda. \tag{10}$$

The radiation-induced current, i_r, for a capacitor, C_T, is

$$i_r = C_T V_p \dot{D}(t) + \sum_n C_T V_{d_n} \int_o^t \dot{D}(\lambda)\, e^{-(t-\lambda)/\tau_{d_n}}\, d\lambda. \tag{11}$$

The first term of Equation (11) is linearly related to $\dot{D}(t)$ and can be handled by most transient circuit analysis programs. The terms appearing in the summation cannot be directly handled in a transient circuit analysis program.

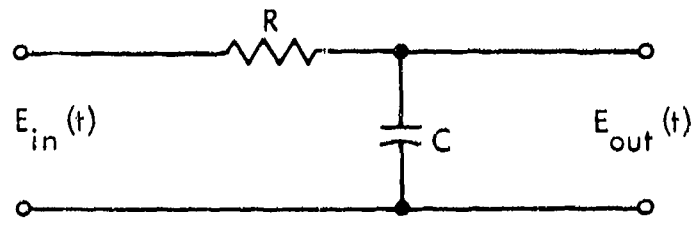

L66-189

Figure 10. R-C Network for Determining Radiation-Induced Transient Currents

However, the similiarity between Equation (10) and the delayed term of Equation (11), shows that if a voltage proportional to $\dot{D}(t)$ is applied to the network in Figure 10, the output voltage is proportional to the delayed current having a τ_{d_n} equal to RC. In general, the delayed portion of the radiation-induced current would be

$$i_{d_n} = C_T V_{d_n} e_{out}(t) \tau_{d_n}, \tag{12}$$

where $e_{in}(t)$ equals $\dot{D}(t)$ and τ_{d_n} equals RC. Note that the units of K_{d_n} and τ_{d_n} must be consistent with the units used in the transient circuit analysis program.

b. Integration

If the delayed term of Equation (11) is rewritten as

$$i_{d_n} = C_T V_{d_n} e^{-t/\tau_{d_n}} \int_0^t D(\lambda) e^{\lambda/\tau_{d_n}} d\lambda, \tag{13}$$

the problem becomes one of evaluating an integral and multiplying it by $C_T V_{d_n} K_{d_n} e^{-t/\tau_{d_n}}$. Since the voltage across the capacitor is proportional to the integral of the current through it, for the circuit in Figure 11, where $i = D(t) e^{t/\tau_{d_n}}$ and C = 1 unit of capacitance.

$$e_C = \int_0^t D(\lambda) e^{\lambda/\tau_{d_n}} d\lambda. \tag{14}$$

And in general

$$i_{d_n} = C_T V_{d_n} e^{-t/\tau_{d_n}} e_C. \tag{15}$$

The two methods described offer a way to analyze and, theoretically, to verify radiation effects on capacitors by using transient circuit analysis programs.

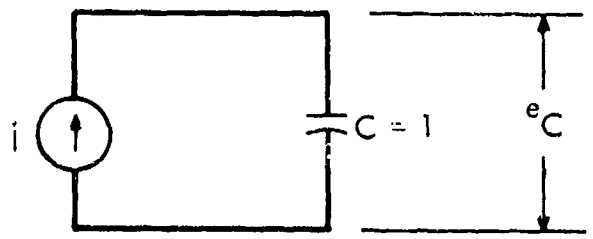

166-190

Figure 11. Capacitor Integration of a Current Source

Furthermore, these methods may be built into existing and future programs as a subroutine without sacrificing flexibility.

5. TEMPERATURE VARIATIONS UNDER LINAC AND AFXR IRRADIATION

In these experiments, the radiation-induced conductivity, as a function of temperature in tantalum-oxide and ceramic capacitors, was investigated at a LINAC and an AFXR. The temperature range selected was from 0°C to 85°C at dose rates between 1.3×10^9 to 9.5×10^{10} rad/s. The induced currents were measured in the two leads of the capacitor to establish the magnitude of charge scattering effects. Charge measurements made for tantalum-oxide were taken in the voltage lead. Charge measurements for ceramic capacitors were not taken because of the usual damped oscillations associated with the current response.

a. Tantalum-Oxide Capacitor Irradiated

The data obtained at LINAC from the exposure of a 1- μF 100-WVdc tantalum-oxide capacitor is shown in Table 10. Pulse widths were varied from 0.3 to 1.5 μs while the voltage applied to the capacitor was held constant at approximately 80 volts. Four temperature settings were chosen between 0°C and 85°C. To compare the effects of LINAC irradiation to AFXR pulses, the same component was exposed to AFXR over the same temperature interval. The voltage applied to the capacitor was again constant and about the same value as at LINAC. However, the pulse width was shortened to approximately 100 ns. The results of the AFXR irradiation are shown in Table 11.

Variations of the radiation-induced current with temperature during testing were explained by a model with the following characteristics:

- A single electron trapping level (E_{n_T}) a few KT below the conduction band

Table 10

TANTALUM-OXIDE CAPACITOR* TEMPERATURE VARIATIONS AT LINAC

t_p (μs)	$\dot{D}$ (10^9 rad/s)	i_{m_1} (mA)	i_{m_2} (mA)
Temperature = 0°C			
0.32	2.29	6.0	5.25
0.51	2.29	10.0	10.0
1.04	1.94	15.25	---
1.04	1.94	15.25	15.50
1.50	1.75	21.0	21.0
Temperature = 20.5°C			
0.31	2.24	9.5	8.8
0.64	1.75	15.5	15.75
1.04	1.75	24.5	---
1.04	1.75	25.0	25.0
1.50	1.81	36.0	36.0
Temperature = 39.4°C			
0.32	1.57	11.5	11.3
0.60	1.45	20.25	20.25
0.65	1.51	20.5	20.5
0.66	1.33	21.0	21.0
1.05	1.39	38.0	38.0
1.57	1.33	---	49.0
1.57	1.33	---	53.0
1.57	1.33	53.0	53.0
Temperature = 83.8°C			
0.32	1.81	26.0	25.0
0.65	1.45	46.0	41.0
1.08	1.39	66.0	66.0
1.57	1.33	94.0	94.0

*1- μF, 100-WVdc capacitor at constant applied voltage of 80.46 volts

--- Represents camera failure or oscillogram response with improper scale settings

Table 11

TANTALUM-OXIDE CAPACITOR*
TEMPERATURE VARIATIONS AT AFXR

Temperature (°C)	$D(10^{10}$ rad/s)	i_{m_1} (mA)	i_{m_2} (mA)	Q_{T_1} (10^{-6} coulombs)
20	7.07	427.0	425.9	3.81
40	6.68	545.0	561.0	4.64
50	8.26	763.6	768.0	6.0
60	6.27	790.0	779.0	5.64
85	7.44	1227.0	1221.0	7.64

Note: Pulse width constant at approximately 100 ns.

* 1-μF 100-WVdc capacitor at constant applied voltage of 79.7 volts: (Same component that was irradiated at LINAC)

- Hole kinetics neglected (holes are assumed to be trapped immediately or to be immobile)

- Recombination at deep lying centers.

In this model an effective mobility is defined (Reference 2) as:

$$\mu^* = \frac{\mu\tau}{\tau + \tau_T} \quad , \tag{16}$$

where τ is the free time an electron spends in the conduction band and τ_T is the time it spends in traps. τ_T is given by

$$\tau_T^{-1} = \nu S_n N_c e^{-E_{n_T}/KT},$$

where

S_n = the capture cross section of an unoccupied trapping center

v = thermal velocity of carriers

N_c = effective density of states in the conduction band

E_{n_T} = trapping energy level

T = temperature (°K)

K = Boltzman's constant (8.63×10^{-5} eV/°K).

The conductivity that will be observed is then given by

$$\sigma = ne\mu^* \tag{17}$$

or

$$\sigma = \frac{ne\mu\tau}{(\tau + \tau_T)} . \tag{18}$$

Assuming $\tau < \tau_T$ and knowing the current density, $J = \sigma E$, one can express the observed radiation-induced current by

$$i = N e^{-E_{n_T}/KT} , \tag{19}$$

where N is a lumped constant possessing a slow temperature dependence compared to the exponential term

$$e^{-E_{n_T}/KT} .$$

The shallow electron trapping level is obtained by plotting log i_m/CVD versus 1/T, the slope being $-E_{n_T}/K$. The data shown in Tables 10 and 11 are used to compare the LINAC and AFXR results (Figure 12). The straight lines are least squares fit to the data. The slopes determined for the LINAC data are essentially constant, (2.17×10^3 °K ± 3%). The slope for the AFXR irradiation is 1.70×10^3 °K. These results imply an average trapping energy level of 0.2 eV for the LINAC and 0.15 eV for the AFXR. The results agree within experimental accuracy.

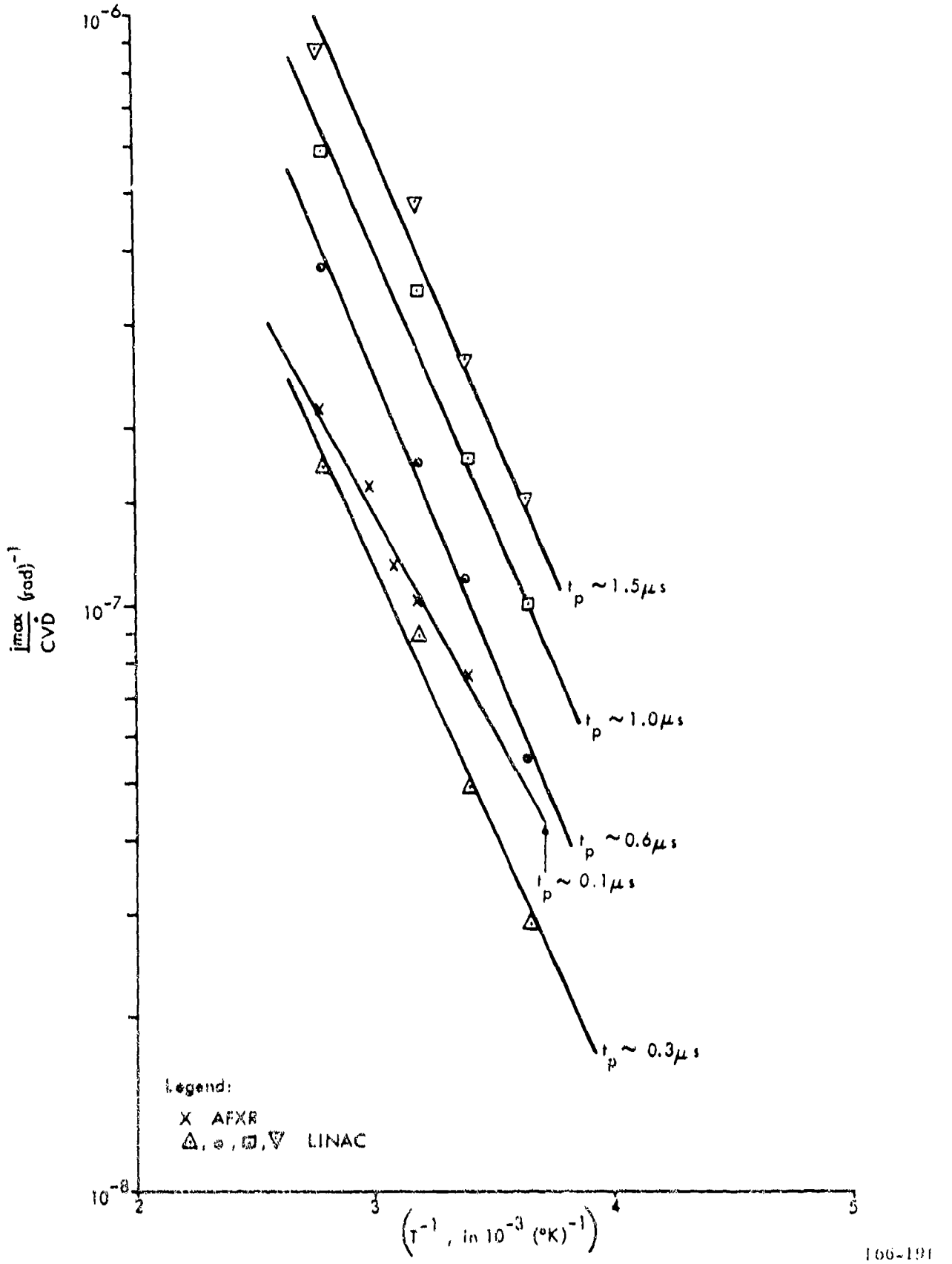

Figure 12. Temperature Variations for a 1- μF 100-WVdc Tantalum-Oxide Capacitor (LINAC and AFXR Tested)

b. Ceramic Capacitors Irradiated

In these experiments, ceramic capacitors of high K-formulation barium-titanate were exposed to radiation at several different sources. The usual response of the ceramic capacitors to the radiation pulse was a prompt portion of radiation-induced current characterized by the usual dielectric model and following the radiation pulse. After the pulse, the ceramic capacitor generated an oscillatory damped mode of constant frequency. This ringing or oscillation is thought to be due to the use of a piezoelectric material as a dielectric. If the component is heated by the pulse in a short time (compared to its thermal-relaxation time), a pressure pulse is developed. The pressure pulse shock excites the unit, causing it to vibrate at its mechanical resonant frequency. This vibration generates the ringing output signal seen in the measuring circuit.

To ensure that these oscillations were not caused by the circuit, different measuring systems were employed with variable circuit parameters. Temperature, applied voltage, and pulse widths were also varied. In each case the period of vibration was constant, whether current probes or sampling resistors were used. This indicates that the oscillations are of dielectric origin and not due to circuit ringing. The results of these experiments are shown in Table 12.

E. CAPACITOR EXCHANGE PROGRAM

1. INTRODUCTION

The present methods for measuring and analyzing transient radiation effects in capacitors consist of applying a semi-empirical equation relating the radiation-induced current to the capacitor dielectric, capacitance, dose-rate, and applied voltage. This equation and its parameters allow a design engineer to predict the magnitude, duration, and circuit history of the radiation effect from capacitors for which data have been tabulated. To ensure that this data tabulation is consistent and accurate, ECOM has established a program of comparative measurements between data taken by General Atomic and IBM on the same components.

The largest source of scatter in the data obtained from irradiation of commercially available capacitors is due to variations in the dielectric material or in the construction of the capacitors. Identically rated capacitors, whose electrical responses are nearly equal, often respond very differently to a radiation burst. This program of comparative testing shows that these variations can be accounted for and brings the data of independent investigators into closer agreement.

Table 12

CHARACTERISTIC OSCILLATIONS IN CERAMIC CAPACITORS

LINAC Data from General Atomic (December 1964, Test)					
Variations				Observed Oscillations	
Pulse	t_p (μs)	T (°C)	V_A (volts)	Period (μ s)	Frequency (10^6 Hz)
Sample 12 — 0.47 μF, 50 WVdc					
3	2	25	15	4.2	0.238
4	2	25	30	4.5	0.222
5	2	25	50	5.0	0.200
Sample 16 — 1 μF, 25 WVdc					
3	2	25	7.5	4.4	0.227
4	2	25	15	4.6	0.217
5	2	25	25	4.5	0.222
6	2	25	0	4.0	0.25
Sample 13 — 2.2 μF, 25 WVdc					
1	2	25	0	4.2	0.238
2	2	25	2.5	4.2	0.238
3	2	25	7.5	4.4	0.227
4	2	25	15	4.4	0.227
5	2	25	25	4.4	0.227
6	2	25	25	4.5	0.222
7	2	25	0	4.5	0.222
LINAC Data from White Sands (December 1965, Test)*					
Sample 56 — 1 μF, 28 WVdc					
2	2	25	23	4.7	0.213
3	1.5	25	23	4.7	0.213
4	1	25	23	4.7	0.213
5	0.5	25	23	4.7	0.213

Table 12. Characteristic Oscillations in Ceramic Capacitors (cont)

AFXR Data from Physics International (March 1966, Test)**					
Variations				Observed Oscillations	
Pulse	t_p (μs)	T (°C)	V_A (volts)	Period (μs)	Frequency (10^6 Hz)
Sample 55 — 1 μF, 25 WVdc					
2	0.1	25	20	4.4	0.227
3	0.1	25	24	4.6	0.217
4	0.1	25	15	4.6	0.217
5	0.1	25	10	4.6	0.217
6	0.1	25	5	4.6	0.217
7	0.1	25	0	4.6	0.217
Sample 53 — 0.1 μF, 50 WVdc					
1	0.1	20	45	4.6	0.217
2	0.1	20	40	4.6	0.217
3	0.1	20	30	4.6	0.217
4	0.1	20	20	4.6	0.217
5	0.1	20	10	4.6	0.217
2	0.1	20	10	4.5	0.222
3	0.1	40	10	4.6	0.217
4	0.1	50	10	4.6	0.217
5	0.1	60	10	4.6	0.217
6	0.1	85	10	4.6	0.217

* Signals were monitored using current probes.
** Signals were monitored using terminators.

2. DATA COMPARISON

Four capacitor samples from General Atomic are listed in Table 13 under General Atomic characterization (Reference 8). To compare the data generated by General Atomic, IBM irradiated the same components at the White Sands LINAC. The results of these tests are discussed below.

a. Mica Capacitors

The radiation-induced current response of mica dielectric capacitors to the LINAC pulse rises to a flat maximum, then drops sharply at the end

Table 13

CAPACITOR DATA FROM GENERAL ATOMIC

Capacitor Type	Rated Capacitance μF	$K_p(10^6 rad^{-1})$	Δ	Sample Number
Foil mica CK5	0.01	16	0.90	61
Silvered mica CRK5	0.01	25	0.94	62
Solid tantalum 150D	1.0	3.6	1.0	24
Solid tantalum 150D	1.0	3.2	1.0	25

of the pulse. This is indicative of a prompt responder characterized by the relation that

$$i_m = K_p CV\dot{D}^{\Delta}, \tag{20}$$

where

K_p = the parameter characterizing the dielectric

C = the capacitance (μF)

V = the applied voltage

D = the dose rate (rad/s)

Δ = a number close to 1 (dependent on the trapping distribution)

i_m = the maximum observed current.

With the assumption that mica is a prompt responder, K_p can also be estimated from Equation (8). The prompt portion of the charge replenished to the capacitor is given by

$$Q_p = K_p CV\dot{D}^{\Delta} t_p. \tag{21}$$

From equations (20) and (21), K_p values were computed (Table 14). The K_p values obtained from current and charge measurements show an average

Table 14

CURRENT AND CHARGE MEASUREMENTS FOR MICA CAPACITORS

Pulse	V_A (volts)	Voltage Side		Burst		Derived Parameters		Difference (%)
		i_m (mA)	Q_T (10^{-6} coulombs)	t_p (μs)	D (10^9 rad/s)	K_p (10^{-6} rad^{-1})	$\frac{Qp}{CVD} - K_p$ (10^{-6})	
Sample 61 — 0.0099 μF, 500 WVdc								
1	0	0.7	*	2.05	3.14	---	---	---
2	199.9	25.8	*	2.05	2.86	6.10	---	---
3	298.6	49.0	1.2	2.05	2.35	6.98	7.4	17
4	466.3	75.0	1.8	2.05	2.28	7.06	8.36	16
5	466.0	72.5	1.7	2.05	2.28	6.82	7.89	14
Sample 62 — 0.010 μF, 500 WVdc								
1	0	1.35	---	2.05	1.36	---	---	---
2	148.5	13.75	---	2.05	1.27	7.28	---	---
3	304.1	23.80	0.54	2.05	1.14	6.89	7.59	9
4	468.4	40.00	0.95	2.05	0.98	8.71	10.2	15
* Camera failure								

difference of about 15 percent. This difference points out that there may be some small delay components that cannot be found in the current measurement because of the resolution of the system. An estimate of the sum of the delayed components is given by the difference in the current and charge measurements:

$$\frac{Q_T}{CVD} - K_p = \sum_n K_{d_n} \tau_{d_n} . \qquad (22)$$

The data in Table 9 show an average difference of 1.19×10^{-6} $(rad)^{-1}$, indicating that mica can be assumed to have a delay component so small that it is not indicated in the current response.

The data in Table 14 show that the maximum induced-current increases linearly with voltage at exposure rates of about 10^9 rad/s. The current magnitudes in Sample 61 are about twice those of Sample 62 because the dose rates differ by a factor of approximately two.

If the dose rate is raised to the power delta obtained by General Atomic, then the K_p values for Samples 61 and 62 are comparable. This comparison is shown in Table 15 and indicates that the difference in characterizations of the same dielectric by two independent investigators may be within the experimental uncertainty associated with the determination of delta.

b. Tantalum-Oxide Capacitors

In addition to the mica capacitors listed in Table 13, two solid tantalum-oxide capacitors were irradiated at the White Sands LINAC and compared to the characterization obtained by General Atomic. The IBM data for this test were presented in Table 10 where pulse widths and temperature were varied at dose rates of around 10^9 rad/s. Temperature is important because an increase in temperature will increase the radiation-induced current.

The data used to compare the General Atomic work are taken at a temperature of 20.5°C. The analytical techniques used to derive the defining parameters of the radiation-induced current are presented in Reference 1. These are the following:

For times greater than the pulse widths ($t > t_p$), the maximum induced current is given by

$$i(t_n) = CV\left[\dot{D}K_d\ \tau_d\left(e^{t_p/\tau_d} - 1\right)\right]\ e^{-t_m/\tau_d} \quad . \tag{23}$$

This expression is used to obtain K_d when the pulse duration t_p is small compared to τ_d. For the narrow LINAC pulses,

$$K_d \sim \frac{i(t_m)\,e^{t_m/\tau_d}}{CV\dot{D}t_p} \qquad \text{for } t_p < \tau_d \text{ and } t \geq t_p \quad . \tag{24}$$

An expression for the time of the maximum current is

$$t_m = \frac{\tau\tau_d}{\tau_d - \tau} \log \frac{\tau_d}{\tau}\left[1 + \frac{\tau - \tau_d}{\tau}\left(\frac{K_p}{K_d\ \tau_d}\right)\right] \quad . \tag{25}$$

Table 15

CHARACTERIZATION OF MICA CAPACITORS

Capacitor Sample Number	General Atomic Numbers		IBM Values (10^{-6} rad^{-1})	
	K_p (10^{-6} rad^{-1})	Δ	K_p	K_p*
61	16	0.90	7.12	17.3
62	25	0.94	8.49	32.4

* K_p value obtained when the dose rate was raised to the power of delta observed by General Atomic

Since K_p is extremely small compared to $K_d \tau_d$, Equation (25) becomes

$$i_m \sim \frac{\tau \tau_d}{\tau_d - \tau} \log \frac{\tau_d}{\tau} . \qquad (26)$$

The only unmeasurable parameters appearing in Equations (24) and (26) are K_d and τ_d. Theoretical values of K_d and τ_d are selected in the time domains of interest and the computed responses are compared to experimental work by means of an automated circuit analysis program (PREDICT). K_p, K_d, and τ_d are adjusted to fit the experimental data (Table 16). Table 16 is still incomplete; however, some agreement can be inferred in the two independent results observed. The power of delta to which the dose rate is raised agrees with General Atomic characterization. The first delay constant τ_{d_1} can be considered to be part of prompt response but can be resolved from the data. Thus, the quantity $K_p + K_{d_1} \tau_{d_1}$ obtained from the IBM data should be comparable to the K_p value found by General Atomic. With this assumption, the data are in agreement.

Table 16

CHARACTERIZATION OF TANTALUM-OXIDE CAPACITORS**

K_p (rads^{-1}) Δ	K_{d_2} (10^{-2} (rad-s)$^{-1}$)	τ_{d_1} (μs)	K_{d_2} (10^{-2} (rad-s)$^{-1}$)	τ_{d_2} (10^{-4}s)	Investigator
3.6×10^{-6} 1	*	*	*	*	General Atomic
5×10^{-7} 1	4.2	0.85	3.6	2	IBM

* Data in the process of being analyzed
** Solid tantalum 150D, 1 μF, 100 WVdc (Sample 24).

Section III

MAGNETIC TESTS

A. INTRODUCTION

The purpose of the magnetic tests was to collect data on the operation of several magnetic devices at high gamma dose rates such as those generated in the prompt portion of a weapon burst. These data will be used to determine if more extensive testing of a variety of magnetic materials should be performed.

To accomplish this task, two types of memory planes with some cores set in each flux state and one type of high-temperature ferrite core were tested in a LINAC electron beam. Also, one type of memory plane with cores set in each flux state, a magnetic recording rotor, two types of magnetic plating test strips, and three types of high-temperature ferrite cores were tested in the X-ray beam of an AFXR.

B. LINAC TESTS

A Gemini memory plane and a Saturn memory plane were statically exposed to a LINAC electron beam. Each core plane had stored information which was read out after exposure to the beam. In addition to the static tests, one type of RCA high-temperature ferrite core was exposed to the electron beam while being either fully selected, half-selected, or disturb half-selected.

1. STATIC TESTS

The Gemini plane, part no. 6144139, consists of 4,096 type T-45 multiaperture (MARS) ferrite memory cores. The type T-45 core is composed of a ferrite material known as 103, type 11. The Saturn plane consists of 8,192 type T-62 toroidal ferrite memory cores. The T-62 core is composed of normal copper manganese.

Each plane was divided into nine sections, and each section contained 100 cores (Figure 13). The memory planes were checked out on the Digital Equipment Corporation 1520 plane/array tester. The output responses of the cores in each section were photographed. Then, the cores were set to the flux states listed in Table 17. The planes were wrapped with a magnetic shielding material to protect the stored information from stray magnetic fields.

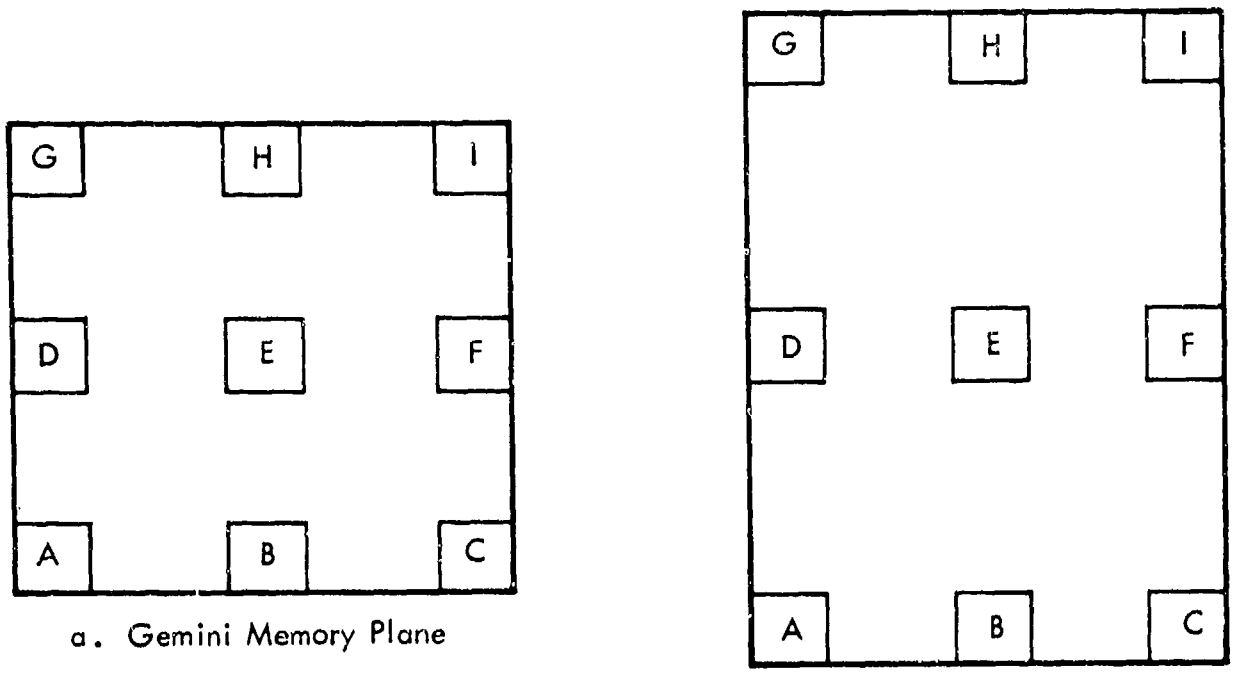

L66-192

Figure 13. Memory Planes

Table 17

FLUX STATES FOR MEMORY ARRAY TESTS

Section	A	B	C	D	E	F	G	H	I
Flux State	1	0	1	0	1	0	1	0	1

Sections G, H, and I of both planes were exposed to a 0.6-μs pulse of electrons. The Saturn plane received total doses of 2900 rad at Section G, 3300 rad at Section H, and 2100 rad at Section I. The peak dose rate was 2.8×10^9 rad/s. The Gemini plane received total doses of 1300 rad at Section G, 900 rad at Section H, and 900 rad at Section I. The peak dose rate was 1.6×10^9 rad/s. Sections A through F in both planes were shielded from the electron beam.

After the memory planes were returned from the test site, the individual sections were read out using the same procedure as for the pre-irradiation checkout. Sections A, B, and C were used as reference sections and were subjected to the same environments as Sections G, H, and I, except for radiation.

Comparison of the oscillograms of the core responses taken before and after irradiation revealed no apparent degradation of the core responses due to the effects of radiation or any other phenomenon.

2. DYNAMIC TESTS

RCA type 264M1 wide-temperature-range ferrite memory cores were exposed to a 10-μs pulse of electrons at an exposure rate in excess of 10^9 rad/s, while operating in each of four switching conditions. Technical data on this core type are shown in Table 18.

Table 18

MEMORY CORE DATA

Parameter	Typical Value
Outside/inside diameter	50/30 mils
Full select current	630 mA
Pulse width	1.5 μs
Output U V_1	80 mV
Output d V_2	12 mV
Switching time	0.90 μs

Five cores were connected in series to increase the signal-to-noise ratio of the output voltage. This gave an output voltage of approximately 400 mV. The axes of the cores and windings were oriented perpendicular to the electron beam.

The cores were operated in the following modes while being exposed to the electron beam:

- Full write, followed by a full read
- Full write, followed by a half-select read
- Full write, followed by two half-select read pulses, then a full read
- Full read, followed by two half-select write pulses, then a full read.

Photos were taken of the core output responses and drive currents in each of the four switching modes before, during, and after irradiation. The output responses and drive currents in the first switching mode were also monitored while the machine was being pulsed, but the electron beam was stopped by an aluminum block in front of the core sample. The purpose of this test was to check for non-radiation problems, such as the r-f field associated with the LINAC. All tests were performed in the test circuit shown in Figure 14.

Comparison of the photos taken before and after irradiation with the photos taken during irradiation showed no apparent degradation of the core responses. TLD dosimetry was not employed for this test. However, by determining the dose rate at the same location for an equivalent current pulse, the dose rate was estimated at 2.7×10^9 rad/s. The oscillograms of the "one" output before, during, and after irradiation are compared in Figure 15.

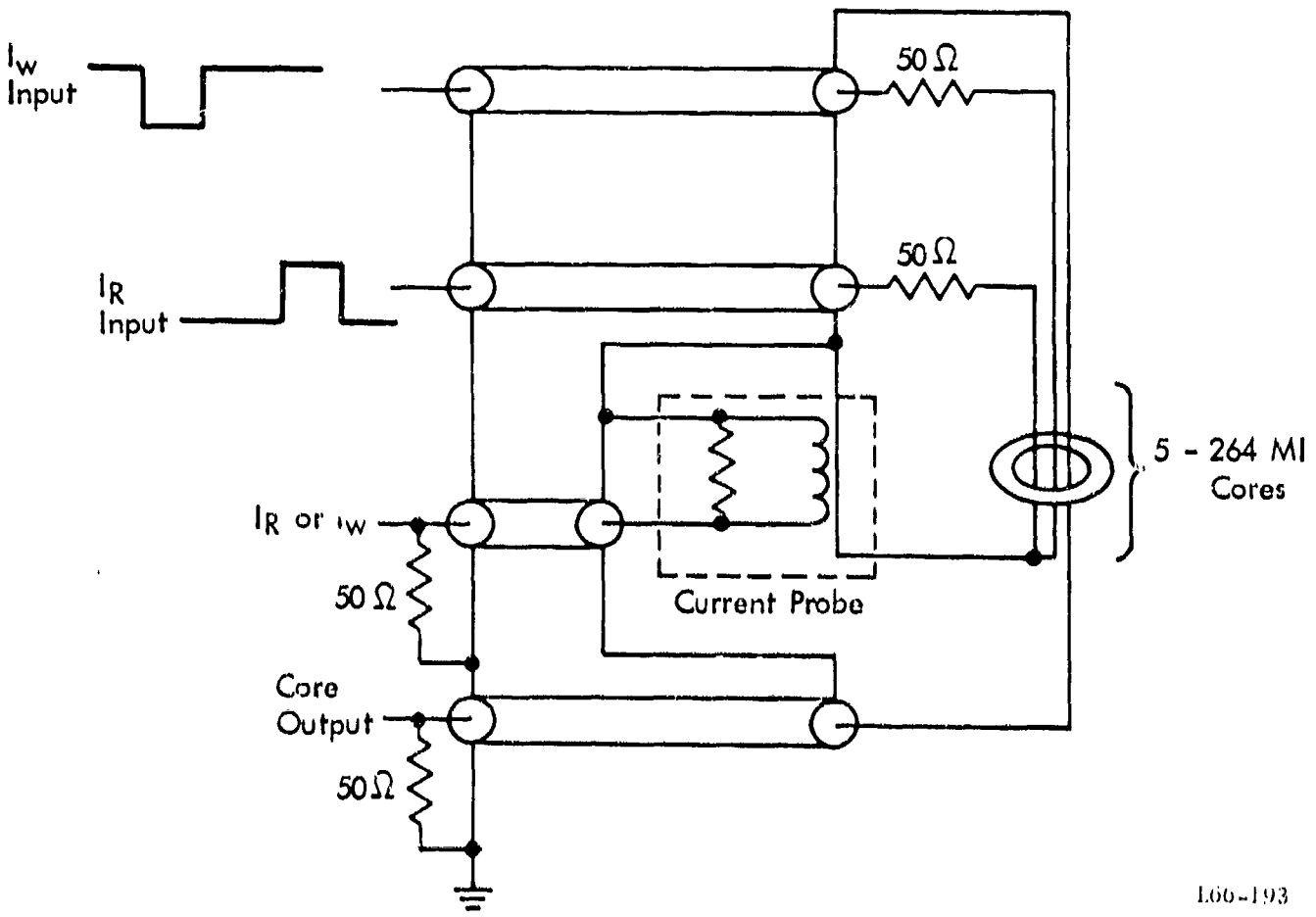

Figure 14. Core Test Circuit

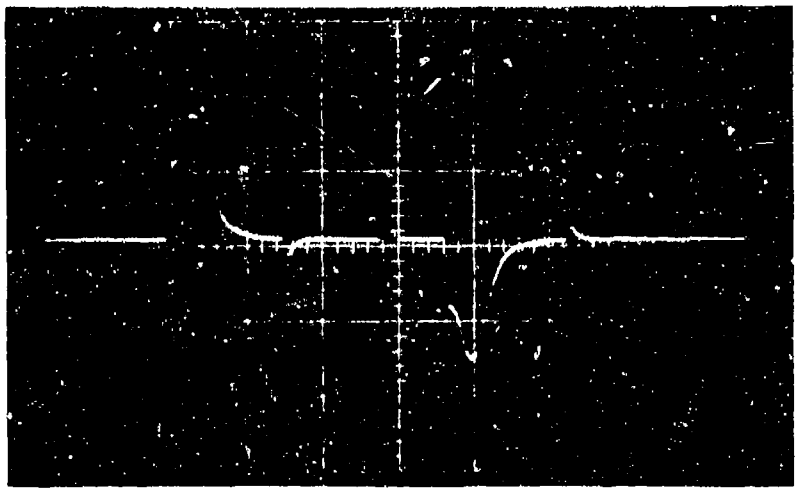

a. Pre-Irradiation

Vertical — 200 mV/Division
Horizontal -- 1 μs/Division

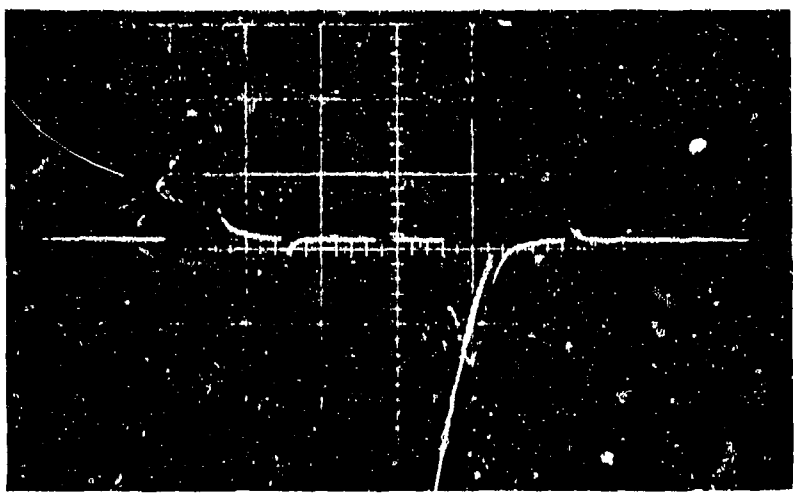

b. During Irradiation

Vertical — 200 mV/Division
Horizontal — 1 μs/Division

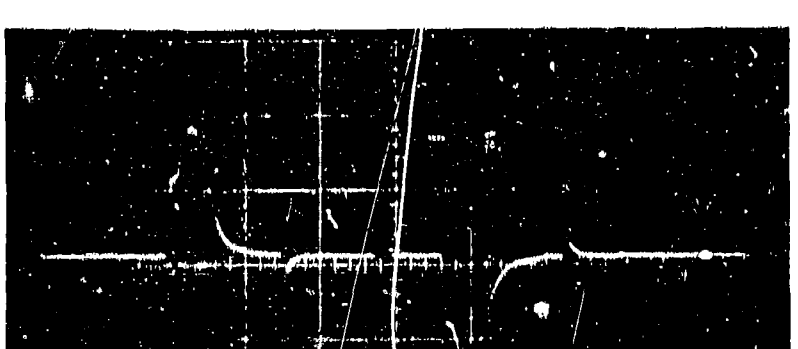

c. Post-Irradiation

Vertical — 200 mV/Division
Horizontal — 1 μs/Division

1166-314

Figure 15. Core Output Responses for a Dose Rate of 2.7×10^9 rad/s

C. AFXR TESTS

A Gemini multi-aperture memory plane, a drum memory recording rotor, and magnetic plating test strips were statically exposed to the AFXR beam. The memory plane and the recording rotor had stored information which was read out after exposure to the X-ray beam. The magnetic plating test strips were tested before and after irradiation to detect any changes of magnetic properties. In addition to the static tests, three types of high-temperature ferrite memory cores were monitored in the AFXR environment while operating in various electrical modes.

1. STATIC TESTS

a. Multi-Aperture Memory Plane

The same Gemini multi-aperture memory plane tested at the LINAC was selected for testing at the AFXR. A second Gemini memory plane was prepared as a reference plane and was packaged with the test plane to detect if the test plane was subjected to any disturbing influence due to shipping, handling, temperature, etc. The two planes received the same environmental conditions except for the radiation exposure.

Each plane was divided into nine sections with information stored in each section. The reference plane had 16 cores per section with "ones" written into every core. The test plane had 100 cores per section with information stored in the pattern shown in Figure 16. The terminations of two x-lines and one y-line were shorted to provide two closed current paths in the x-direction and one closed current path in the y-direction. The shorted windings were used to determine whether the charge scattering effects on current could be enhanced by lowering the external circuit impedance.

The 1/0 section in the center of the plane was the radiation target, with the other sections receiving fringe effects. The divisions of the center section into half "ones" and half "zeros" with both open and shorted drive lines produced eight distinct conditions (Table 19).

The memory planes were checked out on the Digital Equipment Corporation 1520 plane/array tester. The output responses of the cores in each section were photographed. The cores were then set to the indicated flux states.

The test plane was exposed to one AFXR pulse centered at Section E. The dosimetry data is presented in Table 20.

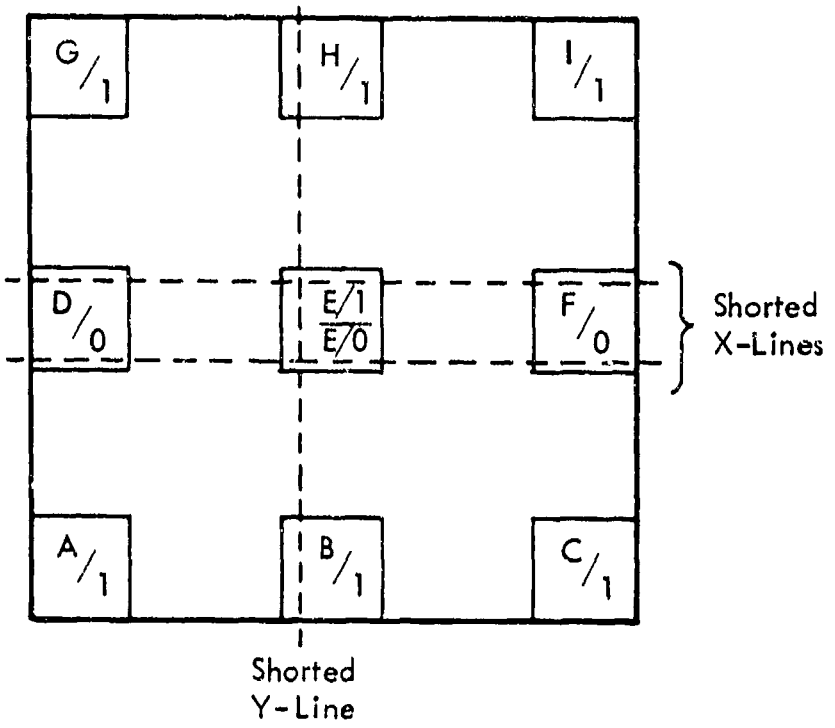

L66-194

Figure 16. Memory Plane Test Configuration

Table 19

MEMORY PLANE TEST CONDITIONS

X-line	Y-line	Hysteresis State	Number of Cores
Shorted	Open	1	9
Shorted	Open	0	9
Open	Shorted	1	5
Open	Shorted	0	3
Shorted	Shorted	1	1
Shorted	Shorted	0	1
Open	Open	1	45
Open	Open	0	27

Table 20

GEMINI MEMORY PLANE DOSIMETRY DATA

Section	$Dose_{(rad)}$	$Dose\ Rate_{(10^{11}\ rad/s)}$
A	2800	0.077
B	3500	0.097
C	3100	0.085
D	3600	1.0
E	4600	1.3
F	4600	1.3
G	4200	1.2
H	5700	1.6
I	4900	1.4

After the memory planes were returned from the test site, the individual sections were read out using the same procedure as for pre-irradiation checkout. Comparison of the pre-irradiation data to the post-irradiation data of the reference plane established that no damage was incurred during routine handling and shipping. Comparison of the pre-irradiation photos to the post-irradiation photos of the test plane gave no indication that the flux state of the cores had been altered due to the effects of radiation.

b. Drum Memory Recording Rotor

A drum memory recording rotor having a nickel-cobalt plating with a coercivity of 225 oersteds was selected for evaluation. Patterns of continuous "ones" were written on 10 tracks across this rotor and on two tracks of a reference rotor. The read-back amplitudes from both rotors were recorded for comparison to the read-backs after irradiation.

The rotor was exposed to an AFXR pulse of 4700 rad at a dose rate of 1.4×10^{11} rad/s at the point on the drum nearest the AFXR tube. The read-back amplitudes of the test drum after irradiation were compared to the read-back amplitudes prior to irradiation in Table 21. Also given are the read-back amplitudes of the reference rotor. Comparison of the pre- and post-irradiation read-backs shows no apparent degradation due to X-ray irradiation at rates as high as 1.4×10^{11} rad/s. The minor discrepancies are within experimental accuracy.

Table 21

RECORDING ROTOR READ-BACK AMPLITUDES

Track Number	Peak-to-peak amplitude (volts)	
	Before	After
Test Rotor - Number 33		
11	10.0	10.0
14	11.0	11.0
20	11.0	10.5
25	11.0	11.0
31	11.0	11.0
35	11.5	11.0
40	11.5	11.0
45	11.5	11.0
55	11.5	11.0
60	11.5	11.0
Reference Rotor - Number 243		
20	11.0	11.0
60	11.0	10.5

c. Magnetic Plating Test Strips

A plating test strip of the same magnetic material as the recording rotor (225 oersteds) and a plating test strip of an experimental material having a coercivity of 690 oersteds were exposed to an AFXR pulse. The 225-oersted material received a 4700-rad pulse at a peak dose rate of 1.4×10^{11} rad/s. The 690-oersted material received a 650-rad pulse at a rate of 1.8×10^{10} rad/s. Since a minimum rate of 10^{11} rad/s was desired, this material was exposed to a second AFXR pulse. This time the test strip received 4500 rad at a rate of $1.2 \times .10^{11}$ rad/s.

Pre- and post-irradiation hysteresigrams of the test strips were compared to detect any changes in the magnetic properties of either material. Neither sample showed any change of coercivity, remanent magnetization, or loop squareness.

2. DYNAMIC TESTS

The behavior of three types of ferrite cores capable of operating over a 100°C temperature range in coincident current memories was investigated in an AFXR environment in various electrical and physical configurations. The tests were designed to show if the high dose rates obtainable from the AFXR can cause a failure and if some configurations are more susceptible than others.

The test apparatus was designed with lead shielding in front of the current probes and in front of the cable ends connected to the test sample. The dose rate at the face of the AFXR tube was less than anticipated so the lead shielding in front of the cable ends was removed to position the test sample at the face of the AFXR tube. Dose rates in excess of 10^{11} rad/s were obtained with this configuration. Operating with the cable ends and test sample socket unshielded increased the amount of material directly in the beam, causing large currents due to charge scattering in the test circuit during the pulse. This test was not designed to determine failure mechanisms or to extrapolate results; however, several inferences can be made from the data obtained.

a. Test Performance and Results

The devices tested were RCA high-temperature ferrite cores, types 264M1, 270M1, and 167M5. A fourth core type, Indiana General MC227, was prepared for testing but was dropped from the test plan because of lack of time at the test facility. Technical data on the four core types is given in Table 22.

Table 22

MEMORY CORE DATA FOR FERRITE CORES

Parameter	Typical Values For the Cores			
	264M1	270M1	167M5	MC227
Outside/Inside Diameter (mils)	50/30	30/18	30/18	50/30
Full Select Current (mA)	630	800	625	700
Pulse Width (μs)	1.5	0.5	0.8	2.5
Output d V_1 (mV)	---	65	50	---
Output u V_1 (mV)	80	---	---	52
Output d V_2 (mV)	12	0	4	8
Switching Time (μs)	0.90	0.41	0.58	1.35

Cores in a coincident current memory are full-selected by simultaneously half-selecting in both the x and y directions. To duplicate this condition, each test sample was wired with an x-winding and a y-winding in series to full-select and operated independently to half-select. The output voltage was monitored across a sense winding. These windings were wound through several cores to increase the output voltage to approximately 200 mV. Ten test samples were prepared for testing in various configurations:

- Sample 1 - Three cores of type 204M1 wound with one x-winding, one y-winding, and one sense winding. The cores were positioned coaxially with the beam.
- Sample 2 - Four cores of type MC227 in the same configuration as sample 1
- Sample 3 - Four cores of type 270M1 in the same configuration as sample 1
- Sample 4 - Five cores of type 167Mb in the same configuration as sample 1
- Sample 5 - Three cores of type 204M1 in the same configuration as sample 1. The cores and the windings were potted with Dow Corning XT-40-110 methyl phenyl siloxane.

- Sample 6 - Three cores of type 264M1 wound with an x-winding, one y-winding, one sense winding, and a fourth winding which was referenced to a d-c voltage. The cores were positioned coaxially with the beam.

- Sample 7 - Core windings arranged identical to sample 1 but without any cores

- Sample 8 - Identical to sample 7 but encapsulated with Dow Corning XT-40-110 methyl phenyl siloxane

- Sample 9 - Three cores of type 264M1 wound with one x-winding, one y-winding, and one sense winding. The axes of the cores were positioned perpendicular to the beam.

- Sample 10 - Three cores of type 264M1 wound with one x-winding, one y-winding, and one sense winding. The x-winding had the length and physical arrangement of a typical multi-level memory. The cores were positioned coaxially with the beam.

Each of these test samples could be tested in any of the following switching conditions:

- Full read, during the AFXR pulse, of cores in the "one" flux state

- Full read, during the AFXR pulse, of cores in the "zero" flux state

- Half-select read, during the AFXR pulse, of cores in the "one" flux state and full read after the occurrence of the AFXR pulse

- Half-select write, during the AFXR pulse, of cores in the "zero" flux state and full read after the occurrence of the AFXR pulse.

The full-select tests were performed in the circuit configurations shown in Figure 17. A half-select pulse was applied through the x- and y-windings connected in series to obtain a full-select drive. Currents were monitored during the AFXR pulse at the points indicated on the diagram. The output voltage was monitored differentially across the cable termination resistors. The test circuit was operated in two physical conditions:

- Condition 1 (R1 = 50 ohms, R2 = 0 ohms) placed the drive windings in the ground side of the drive cable termination, which referenced the drive windings to zero volts

- Condition 2 (R1 = 0 ohms, R2 = 50 ohms) placed the drive windings in the voltage side of the drive cable termination, which referenced the drive windings to the drive potential (e.g., type 264M1 has a drive current of 315 mA; therefore, the drive potential is equal to 315 mA times 50Ω = 15.75 volts).

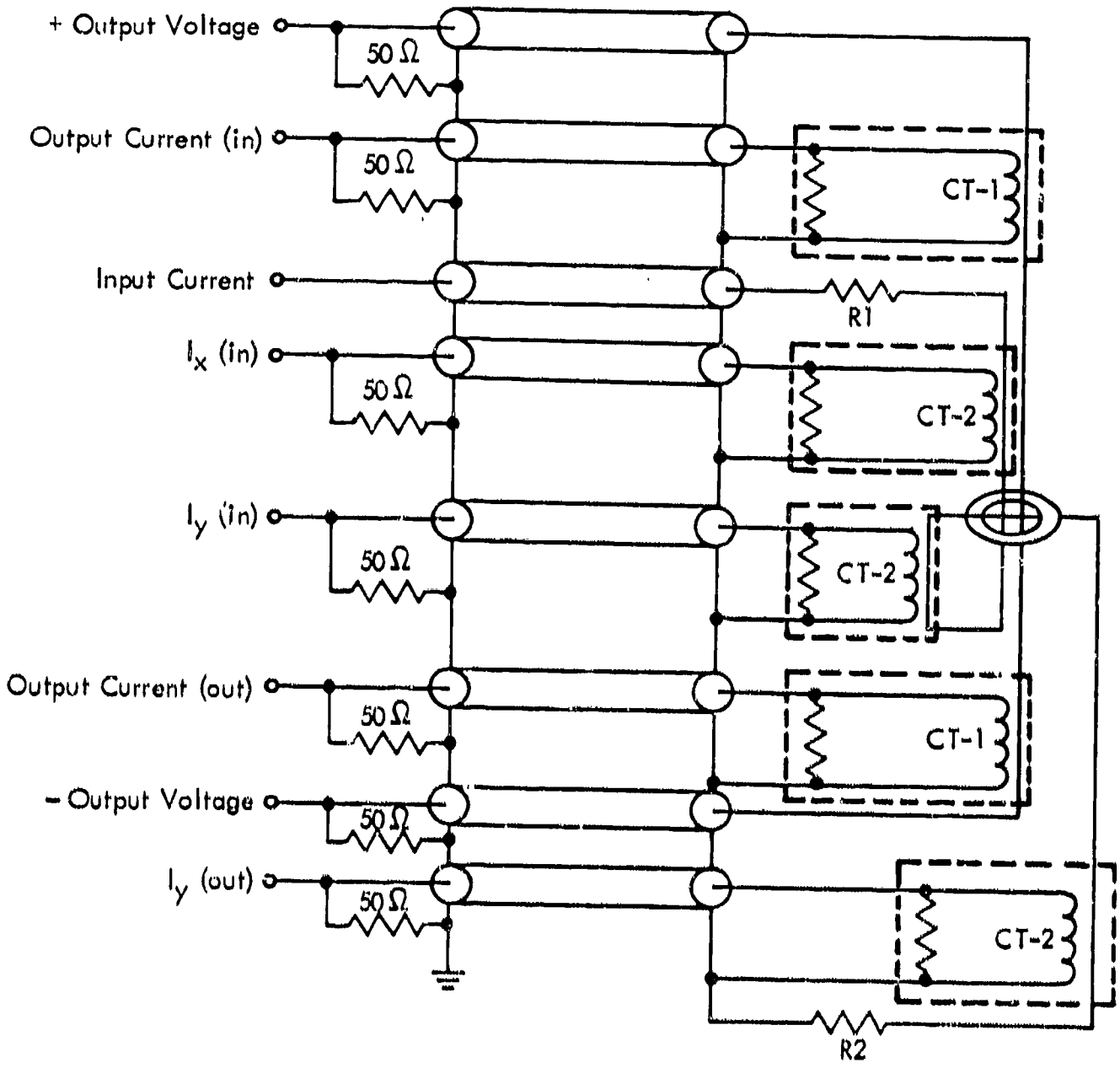

Figure 17. Full-Select Test Circuit

L66-195

The half-select tests were performed in the circuit configuration shown in Figure 18. A half-select pulse was applied to the y-winding during the

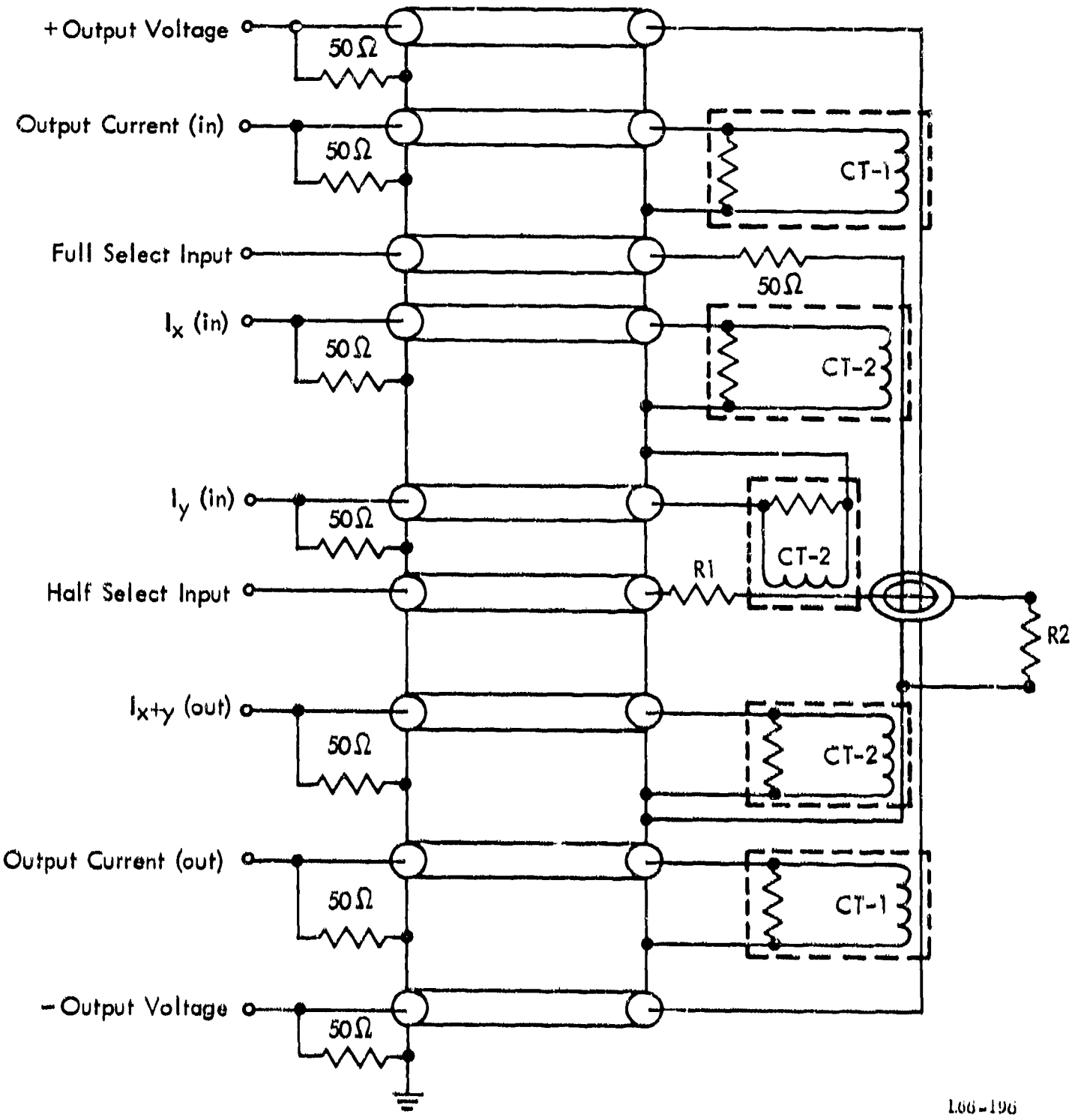

Figure 18. Half-Select Test Circuit

AFXR pulse. The x-winding was used to set the core in the proper flux state and to full read after the pulse. Currents were monitored during the AFXR pulse at the points indicated on the diagram. The output voltage was monitored differentially across the cable termination resistors. This circuit was also operated in the two physical conditions described for the full-select circuit.

The test was performed inside an aluminum R-F shield box positioned against the wall of the exposure room at the beam entrance. A 6-inch-thick lead shield protected the current probes from radiation. The cable ends connected to the cores were shielded by a 2-inch-thick lead shield. Table 23 lists the tests performed in this configuration and the dosimetry data for each.

Table 23

CIRCUIT TEST DESCRIPTION WITH CABLE ENDS SHIELDED

Sample Number	Test Description	Drive Winding Reference	Dose (rad)	Dose Rate (10^{10} rad/s)
1	Full-select read, during	Ground	2200	6
9	AFXR pulse, of cores	Ground	2500	7
5	in "one" flux state	Ground	1200	3.4
7	Full-select read, during	Ground	1600	4.2
8	AFXR pulse, of core windings	Ground	2300	6

Currents due to charge scattering were observed in all leads; however, no core switching failures were observed. The currents observed in the samples without cores were comparable to the currents observed in the samples with cores. The currents observed in the potted samples were comparable to the currents observed in the samples which were not potted.

The lead shield in front of the cable ends was removed to allow the samples to be positioned closer to the AFXR tube to obtain higher dose rates. Table 24 lists the tests performed in this configuration.

In each case, the cores exhibited the proper output during and after the AFXR pulse. Current due to charge scattering was observed in every lead. The currents observed in the samples without cores were comparable to the currents observed in the samples with cores. Exposure of the test fixture without a sample plugged in indicated that approximately half the current originated in the test fixture. When the drive windings were referenced to ground, the current in the lead connected to ground was much

Table 24

CIRCUIT TEST DESCRIPTION WITH CABLE END SHIELD REMOVED

Test Description	Sample Number	Drive Winding Reference	Dose (rad)	Dose Rate (10^{11} rad/s)
Full-select read, during the	1	Ground	6500	1.8
AFXR pulse, of cores in the	1	Drive potential	5800	1.6
"one" flux state	5	Drive potential	5300	1.6
	10	Ground	4800	1.3
Full-select read applied	7	Drive potential	4700	1.3
to core windings during the				
AFXR pulse				
Full-select read, during the	1	Ground	5400	1.7
AFXR pulse, of cores in the	9	Ground	5800	1.5
"zero" flux state				
Half-select read, during the	1	Ground	3600	1.2
AFXR pulse, of cores in the	9	Ground	4300	1.2
"one" flux state	5	Ground	8500	2.4
	10	Ground	7300	2.0
	3	Ground	4300	1.2
	3	Drive potential	4600	1.2
	4	Ground	4200	1.2
	4	Drive potential	5400	1.3
Half-select read applied	7	Ground	4600	1.2
to core windings during the	7	Drive potential	4300	1.2
AFXR pulse				
Half-select write, during the	3	Ground	3700	1.0
AFXR pulse, of cores in the	3	Drive potential	4900	1.4
"zero" flux state	4	Ground	4200	1.2
Test fixture without		Drive potential	3900	1.1
a sample				

larger than the lead connected to the generator through the termination resistor. When the drive winding was referenced to the drive potential, the currents in both leads were comparable. This appeared to be due to the matched impedance to ground (the 50-ohm termination in one lead and the 50-ohm generator impedance in the other lead) rather than the presence of the drive voltage, because the sense winding always had a matched impedance to ground and currents comparable to each other.

Since the core switching was not influenced by the AFXR beam at dose rates available in the exposure room, the IBM shield box and the front wall of the exposure room were removed to permit a higher dose rate by positioning the core samples against the face of the AFXR tube. The extremely high R-F noise level with this configuration did not permit data recording during the AFXR pulse. The following is a description of the tests performed and the effects observed under these conditions. All tests were performed with Sample 3.

While set to the "one" flux state, the core was half-select read during the AFXR pulse. Post-irradiation read-out revealed that the "one" stored in the core was destroyed. The dose was 10,800 rad at a peak dose rate of 3×10^{11} rad/s. Figure 19 compares the "one" output recorded before the pulse to the output recorded after the pulse.

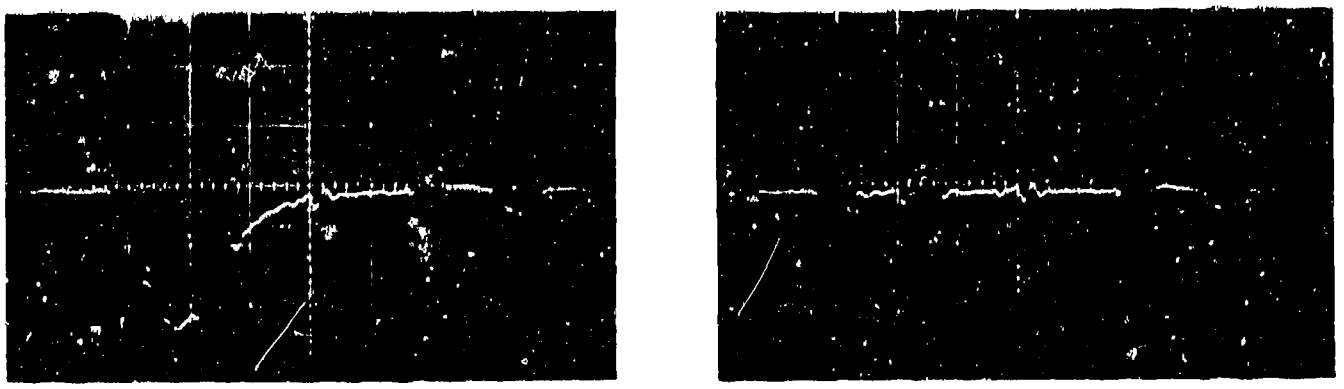

a. Pre-Irradiation

Vertical — 100 mV/Division
Horizontal — 100 ns/Division

b. Post-Irradiation

Vertical — 100 mV/Division
Horizontal — 100 ns/Division

Figure 19. Core Output Response of a "one" Output Before and After 10,800 rad 1160-315

The above test was repeated to verify that the stored information was not lost due to a mistake in the procedure or due to a freak occurrence. The stored "one" was destroyed during the AFXR pulse. The dose was 8100 rad at a peak rate of 2.2×10^{11} rad/s. Figure 20 compares the "one" output recorded before the pulse to the output recorded after the pulse.

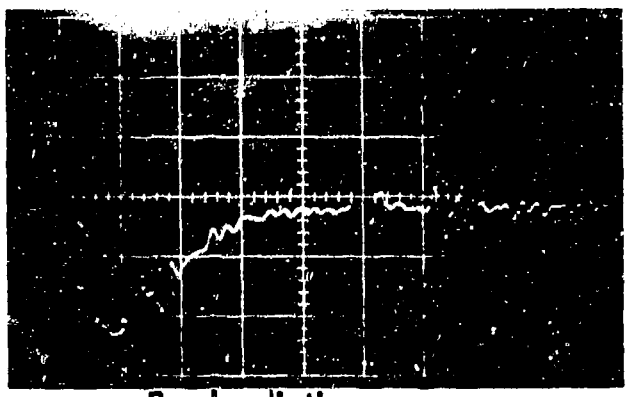

a. Pre-Irradiation

Vertical — 100 mV/Division
Horizontal — 100 ns/Division

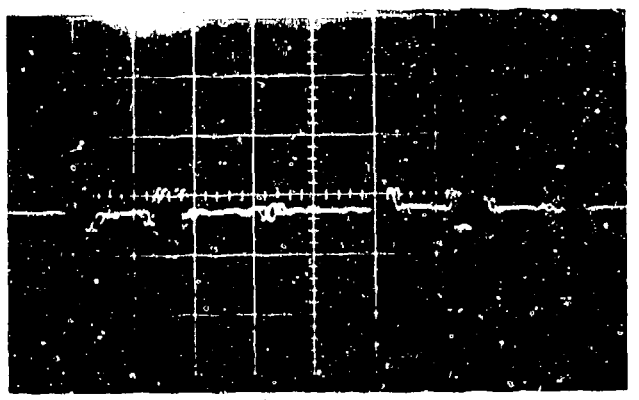

b. Post-Irradiation

Vertical — 100 mV/Division
Horizontal — 100 ns/Division

Figure 20. Core Output Response of a "one" Output Before and After 8100 rad

H66-316

With the cores in the "zero" flux state a half-select write was applied during the occurrence of the AFXR pulse. Post-test read-out revealed that a "one" was partially written into the core. The dose was 10, 000 rad at a peak dose rate of 2.7×10^{11} rad/s. Figure 21 is the comparison of the "zero" output recorded before the pulse to the output recorded after the pulse.

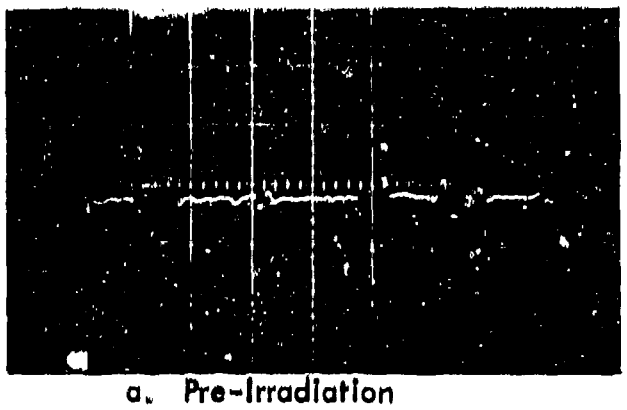

a. Pre-Irradiation

Vertical — 100 mV/Division
Horizontal — 100 ns/Division

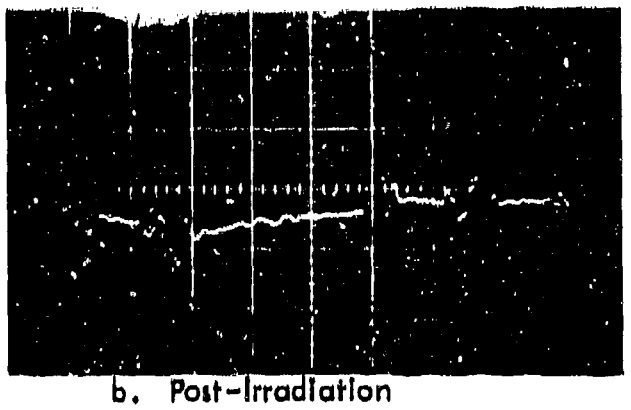

b. Post-Irradiation

Vertical — 200 mV/Division
Horizontal — 100 ns/Division

Figure 21. Core Output Responses of a "zero" Output Before and After 10, 000 rad

H66-317

The core was set to the "one" flux state, then exposed to an AFXR pulse. Post-irradiation read-out revealed that the "one" was destroyed. The dose was 8600 rad at a peak dose rate of 2.4×10^{11} rad/s. Figure 22 compares the "one" output recorded before the pulse to the output recorded after the pulse.

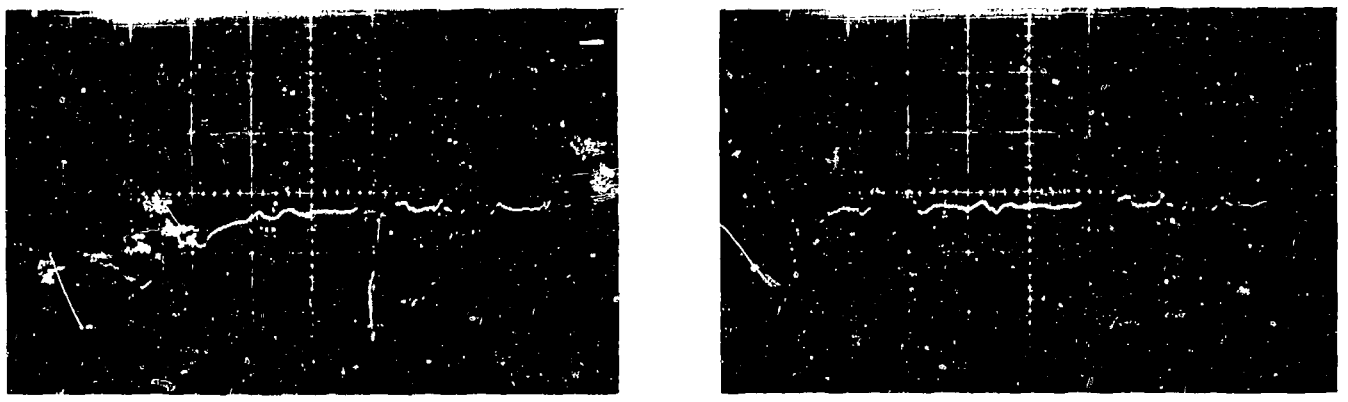

a. Pre-Irradiation

Vertical — 200 mV/Division
Horizontal — 100 ns/Division

b. Post-Irradiation

Vertical — 200 mV/Division
Horizontal — 100 ns/Division

Figure 22. Core Output Response of a "one" Output Before and After 8600 rad

H66-318

The core was definitely failing at dose rates only slightly higher than the rates received inside the shield, where no failures were observed. The core was set to the "one" flux state and exposed to an AFXR pulse at a dose rate equal to the rate received inside the shield. Post-irradiation read-out revealed that the "one" was destroyed. The dose was 6000 rad at a peak dose rate of 1.7×10^{11} rad/s. Figure 23 is the comparison of the "one" output recorded before the pulse to the output recorded after the pulse.

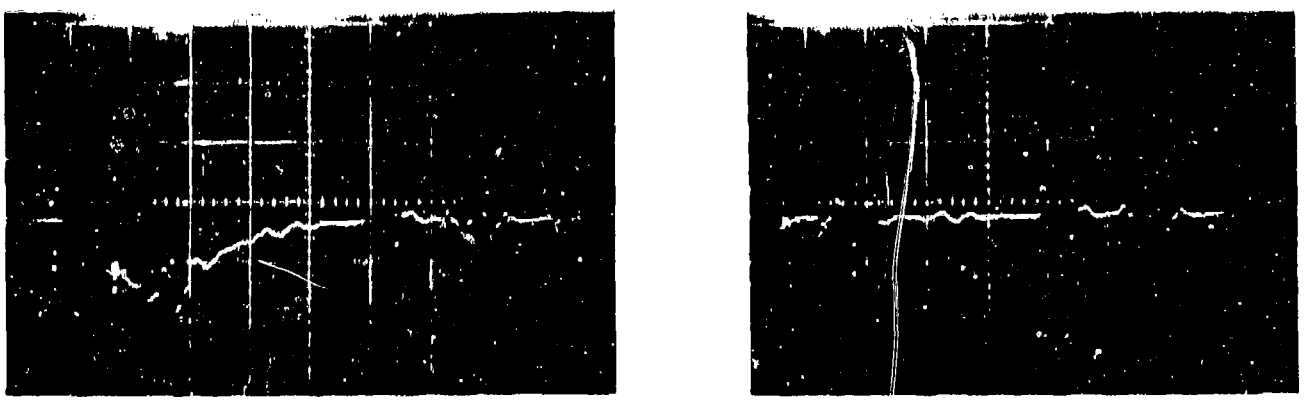

a. Pre-Irradiation

Vertical — 200 mV/Division
Horizontal — 100 ns/Division

b. Post-Irradiation

Vertical — 200 mV/Division
Horizontal — 100 ns/Division

Figure 23. Core output Responses of a "one" Output Before and After 6000 rad

H66-319

The core was set to the "zero" flux state and exposed to one AFXR pulse. Post-irradiation read-out showed the "zero" output after irradiation to be identical to the "zero" output before irradiation. The dose was 10,600 rad at a peak dose rate of 3×10^{11} rad/s.

Stored information was destroyed at dose rates between 1.7×10^{11} and 3×10^{11} rad/s in the combined X-ray and r-f environment. When the r-f noise was shielded, the cores switched properly at dose rates as high as 2.4×10^{11} rad/s. To establish r-f noise, and not the AFXR pulse, as the cause of core failures, several full-select and half-select tests were repeated inside the aluminum shield box. The cores switched properly at dose rates between 1.7×10^{11} and 2.1×10^{11} rad/s. Results show that the observed failures were not caused by the X-ray pulse.

b. Failure Mechanisms

The most obvious mechanisms which might induce a core failure are those associated with air ionization and charge scattering. Because of the small dimensions of typical cores (< 0.01 cm^2 section), failures due to charge scattering from the cores alone would be expected at dose rates far in excess of those in the actual test. However, if the dimensions of a core plane and its connectors are considered, the above statement may no longer be valid.

In the test, signals of the order of 100 mA at 2×10^{11} rad/s resulted. Since the currents measured in both leads to the sense winding were of the same polarity, these currents were attributed to charge scattering effects. The polarity of these currents indicates that electrons were being scattered out of the core, the core winding, and the test fixture. Assuming a charge scattering coefficient of approximately 1 picocoulomb per rad-cm^2, and considering the cross-sectional areas of the test fixture, core windings, and cores (~ 1 cm^2), the size of currents measured are consistent with currents expected from charge scattering.

The 264M1 test core is normally switched by a 0.6-A pulse approximately 1.5 μs wide. Since the radiation-induced currents only lasted approximately 0.1 μs, a direct estimate of a failure level was not possible. To determine the effect of a narrower, more intense pulse, bench measurements were made of the input current versus the pulse width necessary to switch the core. During the test, the pulse width was held constant and the input current was varied until the output voltage waveform was similar to that for the 1.5-μs case. Approximately 1.4 A was required to switch the core, with a 0.1- μs pulse. This would indicate that core failures due to charge scattering off the core winding, the test fixture, and the core are likely to result at dose rates approaching 10^{12} rad/s.

Although no core failures attributable to the radiation pulse were observed, losses of core-stored information could possibly result at dose rates higher than 10^{11} rad/s. Cores requiring less current for switching at these pulse widths would be even more sensitive. In an operational configuration, the dose rates which might cause loss of core-stored information would be determined by the current necessary to switch the cores and by the packaging of the core.

D. CONCULSIONS

These tests showed that the radiation from either a LINAC or AFXR machine does not affect information stored in cores and other magnetic devices. No significant additional data will be obtained until dose rates at least 10^{12} rad/s are available at a distance from the source sufficient to allow adequate shielding of the test instrumentation.

Section IV

DOSIMETRY

A. INTRODUCTION

The dosimetry associated with the SPRF, the LINAC, and the AFXR radiation tests is discussed in this section. The dosimetry techniques employed have been detailed (References 1 and 2). Only the dosimetry pertinent to the tests conducted under this contract will be summarized here.

Standard dosimetry techniques were used, except for the SPRF experiments, in which the neutron-to-gamma-ray flux was altered, and the LINAC tests, in which special precautions were observed regarding sample geometry. The exceptions will be treated in detail. The standard techniques include the following.

1. GAMMA DOSIMETERS

Silver-activated glass fluorods or lithium-flouride thermo-luminescent dosimeters were used for gamma dose determinations. These dosimeters were calibrated at a Colbalt-60 radioisotope source against secondary standard Landsvork roentgen chambers. At the SPRF, lithium shields enclosed the glass rods.

2. NEUTRON DOSIMETERS

The SPRF dosimetry group supplied all the neutron fluence data. These data were derived from a set of threshold dosimeters: plutonium, neptunium, uranium, sulfur, and gold. The standard neutron energy thresholds for these dosimeters are >10 keV, >0.6 MeV, >1.5 MeV, >0.3 MeV, and <0.4 eV, respectively. Plutonium fluences are reported in this document.

B. DOSE RATE DETERMINATIONS

1. GAMMA RATE DETERMINATION

In all cases, gamma dose rates were determined from the dose (D) observed by a gamma dosimeter located on a component, and a remote detector signal (current), I(t). Dose rates were calculated from the relation

$$\dot{D}(t) = DI(t)/Q, \qquad (27)$$

where Q is the time integral of I(t).

I(t) was obtained from a silicon PIN diode, a phosphor-photodiode, and an aluminum block, at the SPRF, AFXR, and LINAC, respectively. At the SPRF, the PIN was placed on a common arc with the components; at the AFXR, the detector was placed directly behind the test samples; and at the LINAC, the block stopped that portion of the electron beam which was not to strike the components under test.

2. NEUTRON FLUX DETERMINATIONS

At the pulsed reactor, neutron fluxes $\dot{N}(t)$, were derived from the relation

$$\dot{N}(t) = NI(t)/Q_p, \tag{28}$$

where N is the neutron fluence and Q_p is the time integral of I(t) over the prompt portion of the reactor pulse. [p]This assumes that the neutron fluence decays very rapidly after the peak of a burst.

This approximation is required because of the lack of a pure neutron-sensitive (gamma-insensitive) detector, and the lack of information regarding the histories of relative neutron-to-gamma-ray time during a reactor burst.

C. ALTERATION OF NEUTRON-TO-GAMMA RATIO

At the SPRF, the neutron-to-gamma-ray ratio of several bursts was altered using various polyethylene and lead shield combinations (Reference 9). The test setup for those tests is illustrated in Figure 24. Polyethylene was used to degrade the intensity of the neutron flux without significantly altering the gamma ray flux. Lead degraded the gamma ray flux without significantly degrading the neutron flux. Figure 25 illustrates the neutron fluence variation versus the gamma dose obtained during the test series. Note that the fast neutron spectrum was not significantly altered during the test.

D. LINEAR ACCELERATOR TESTS

Because direct electron irradiations were performed, precautions were necessary to assure maximum uniformity of dose deposition in test samples. The precautions were necessary for two reasons:

- The short range of the electrons limit the depth of test samples.
- The electron beam spatial distribution limits the dose rate uniformity of samples transverse to the beam direction.

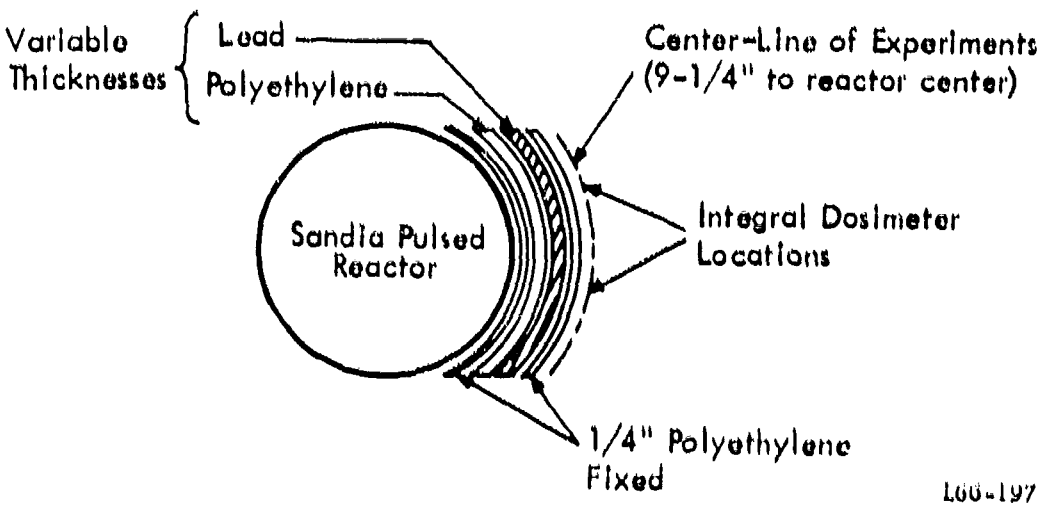

Figure 24. Experimental Arrangement for Neutron and Gamma Sensitivity Test

The dose (D) delivered to a thin sample by an electron beam is given by the relation:

$$D = -\frac{1}{\rho}\frac{dE}{dX} \cdot 10^{11} \cdot Q, \qquad (28)$$

and this dose is delivered at a rate

$$\dot{D} = -\frac{1}{\rho}\frac{dE}{dX} \cdot 10^{11} \cdot J, \qquad (20)$$

where,

$-\frac{1}{\rho}\frac{dE}{dX}$ = the material stopping power in MeV -cm^2/gm,

J = the beam current density in amp/cm^2

Q = the total charge delivered in coul/cm^2

The range (R_0) of these electrons is

$$R_0 \doteq E_0/2.8 \text{ gm/cm}^2 \qquad (30)$$

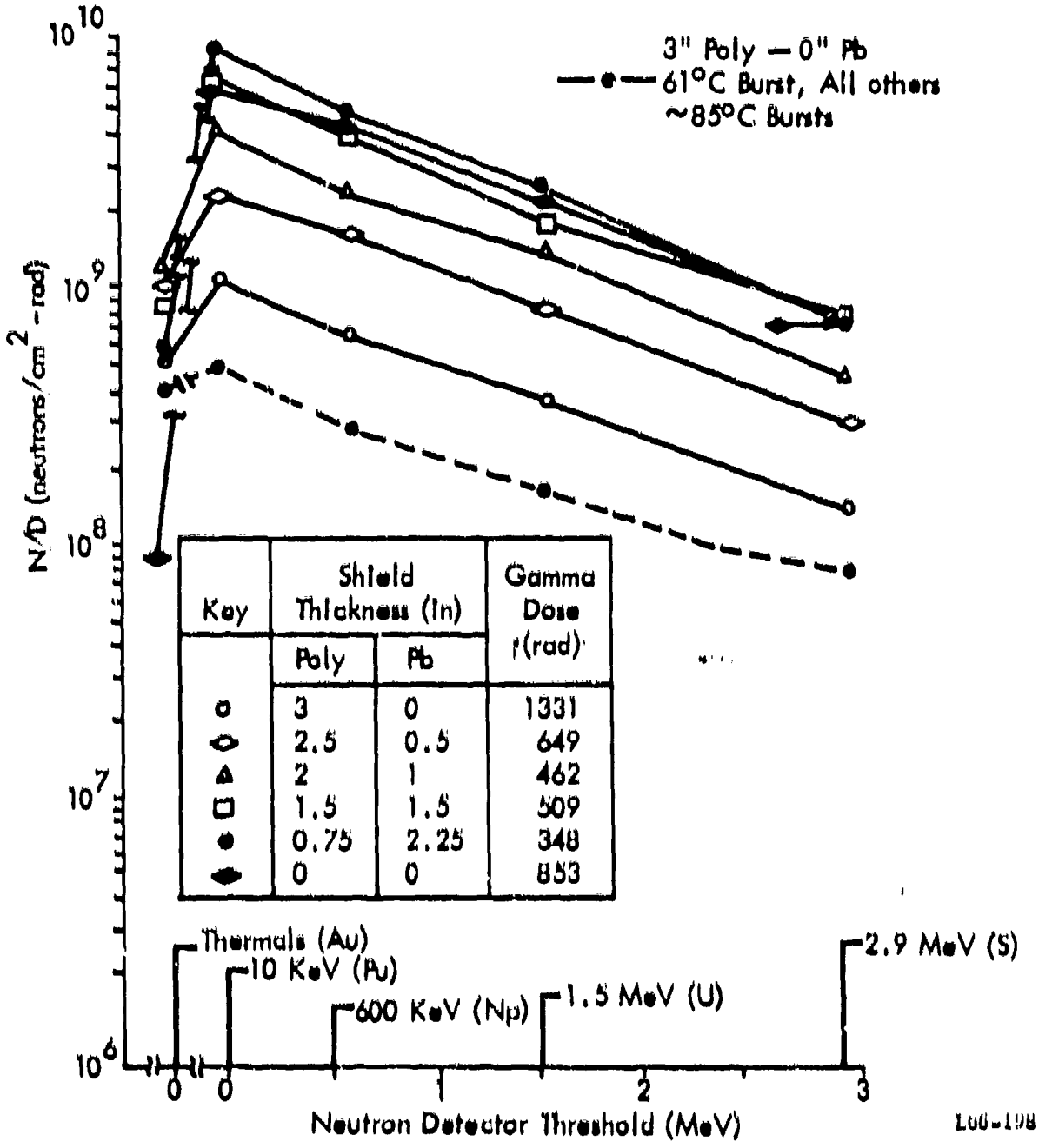

Key	Shield Thickness (In)		Gamma Dose r(rad)
	Poly	Pb	
○	3	0	1331
◇	2.5	0.5	649
△	2	1	462
□	1.5	1.5	509
●	0.75	2.25	348
⬬	0	0	853

Figure 25. Neutron Spectra for Various Shielding with Gamma Dose Normalization

to within 20 percent in the energy interval, $1 < E_0 < 100$ MeV, where E_0 is the energy of incident electrons. In actual practice, the dose in a material is a function of the depth of the material (Figure 26).

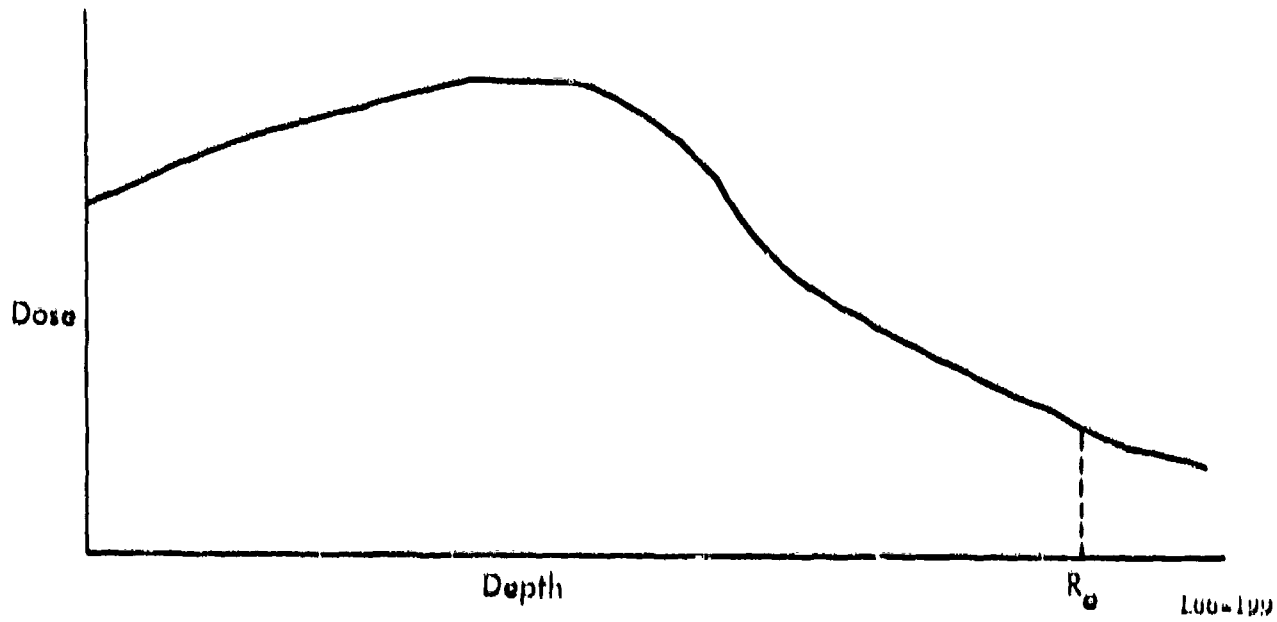

Figure 26. Electron Irradiation Dose as a Function of Depth

To avoid large differences in dose, the maximum depth of test samples was restricted to $R_0/2 = E_0/4$ gm/cm^2 in the LINAC tests. Differences in dose rate perpendicular to the direction of the beam had to be minimal. From Equation (20), spatial variations in beam current density (J) will cause different dose rates across a sample in the LINAC electron beam. In Reference 10, the following formula is derived, relating the peak dose rate ($\dot{D}$), beam current (I_B), sample length (1 cm), and dose rate non-uniformity parameter (β), for a Gaussian beam current distribution:

$$I^2\dot{D}/I_B = \frac{4 \times 10^{11}}{\pi} \left(-\frac{1}{\rho}\frac{dE}{dX}\right) \log (1/\beta). \qquad (31)$$

Beta (β) is the ratio of the dose rate at the edge of the sample to the peak dose rate at the center of the sample. For materials with atomic numbers between 3 and 80, and for electron energies between 1 and 100 MeV,

$$-\frac{1}{\rho}\frac{dE}{dX} = 1.5 \pm 0.5 \ \frac{\text{MeV} - \text{cm}^2}{\text{gm}} . \qquad (32)$$

Thus,

$$\frac{l^2 D}{I_B} = 1.91 \times 10^{11} \log\ (1/\beta). \tag{33}$$

Equation (33) illustrates the correlation of sample size and peak dose rate when using direct electron beam irradiations.

For the LINAC tests, the maximum length of test samples was 2.5 cm, β was chosen to be 0.8 to assure a ± 10 percent dose uniformity across the largest test samples, and a maximum I_B of 0.5 A was achieved. Equation (33) predicts a maximum dose rate of 1.5×10^9 rad/s for this case.

Although the above equation was useful for planning the LINAC tests and setting instrumentation scale factors, dosimetric beam maps were still necessary at the test sites to establish dose rate profiles for each particular accelerator. This was done using a lithium-fluoride thermo-luminescent dosimeter. The observed peak dose rates, corresponding to a β of 0.8, agreed with the result from Equation (33). Extensive instrumentation scale factor changes at the test site were thereby avoided.

One further precaution was observed at the test site. To avoid errors caused by the scattering of electrons, dosimeters were attached to the sides rather than to the front or rear of the irradiated components. For the larger components, the dose rates obtained from the dosimeters were lower than the mid-beam dose rates by a factor of 0.8. The error was less for the smaller components, as was the dose rate non-uniformity.

REFERENCES

1. Frankovsky, F. A. and Shatzkes, M. "Reactor and Linear Accelerator Induced Effects in Dielectrics," IBM Report No. 66-825-1944, March 1966, Owego, New York.

2. Frankovsky, F. A. "Study of Effect of High-Intensity Pulsed Nuclear Radiation on Electronic Parts and Materials (SCORRE)," Quarterly Report No. 3, IBM Report No. 66-621-6 (ECOM-00212-6), April 1966.

3. TREE Handbook, DASA 1420, Battelle Memorial Institute, Columbus, Ohio, pp G-1 to G-11.

4. "Survey of Irradiation Facilities," REIC Report No. 7, Battelle Memorial Institute, Columbus, Ohio, pp. 25, 26.

5. Colp, J. L. and O'Brien, P. D. "The Sandia Pulsed Reactor Facility," SCR-220.

6. "Study of Effect of High-Intensity Pulsed Nuclear Radiation on Electronic Parts and Materials (SCORRE)," Quarterly Report No. 1, IBM No. 66-521-10 (ECOM-0012-3).

7. "Automated Digital Computer Program for Determining Responses of Electronic Systems to Transient Nuclear Radiation," Vol. III - TREAT Component Analysis Program, IBM Report No. 64-621-6, July 1964.

8 Nichols, D. I., Overmyer, R. F., and VanLint, V. A. J. "Radiation Effects on Dielectric Materials," Quarterly Report, General Atomic Report No. GA-6715 (ECOM-01412-1).

9. Martin, J. A. "Electron Beam Radiation Tests . . . Maximum Dose Rate Versus Sample Size," IBM Report No. 66-825-1761, June 1966.

10. Kloepper, R. M., Martin, J. A., and Shatzkes, M. "Neutron and Gamma Sensitivities of Dynamic Detectors," IEEE Transactions in Nuclear Science, Volume NS-12 No. 5, October 1965, p. 101.

DOCUMENT CONTROL DATA - R&D

(Security classification of title, body of abstract, and indexing annotation must be entered when the overall report is classified)

1. ORIGINATING ACTIVITY (Corporate author)
IBM Corporation, Federal Systems Division
Electronics Systems Center
Owego, New York

2A. REPORT SECURITY CLASSIFICATION
Unclassified

2B. GROUP

3. REPORT TITLE
STUDY OF EFFECT OF HIGH-INTENSITY PULSED NUCLEAR RADIATION ON ELECTRONIC PARTS AND MATERIALS (BOORE)

4. DESCRIPTIVE NOTES (Type of report and inclusive dates)
Final Report (16 June 1964 to 15 July 1966)

5. AUTHOR(S) (Last name, first name, initial)
Boezar, Paul G.
Boyd, Gilbert E.
Cordwell, Wayne A.
Frankovsky, Frank A.

6. REPORT DATE	7a. TOTAL NO. OF PAGES	7b. NO. OF REFS.
October 1966	86	10

8a. CONTRACT OR GRANT NO.
DA28-043 AMC-00212(E)
b. PROJECT NO.
c. 5001.21.700.01
d.

9a. ORIGINATOR'S REPORT NUMBER(S)
66-521-13

9b. OTHER REPORT NO.(S) (Any other numbers that may be assigned this report)
ECOM-00212-F

10. AVAILABILITY/LIMITATION NOTICES

11. SUPPLEMENTARY NOTES
DASA Supported

12. SPONSORING MILITARY ACTIVITY
U. S. Army Electronics Command
Fort Monmouth, New Jersey
AMSEL-KL-EC

13. ABSTRACT

This report describes the radiation-induced behavior of tantalum-oxide, mica, ceramic, Mylar, glass, and polystyrene capacitors using results obtained at several sources. Also included are discussions of the following:

- Experimental techniques at each radiation source, including measurement of circuits, components, dosimetry, and variation of circuit and radiation parameters
- Results from SPR II, LINAC, and ASTR tests describing the dependence of the induced current for the metallized dielectric
- Interpretation of these results in terms of appropriate models and radiation and circuit parameters
- Comparison of the effects observed at each irradiation source
- Description of the tests on magnetics and the test results.

Adapted From
DD FORM 1 JAN 64 1473

14. KEY WORDS	LINK A		LINK B		LINK C	
	ROLE	WT	ROLE	WT	ROLE	WT
Nuclear Radiation Effects Pulse Radiation Effects Radiation Effects in Electronic Parts and Materials Radiation Effects in Capacitors and Memory Cores						

INSTRUCTIONS

1. ORIGINATING ACTIVITY: Enter name and address of the contractor, subcontractor, grantee, Department of Defense activity or other organization (corporate author) issuing the report.

2a. REPORT SECURITY CLASSIFICATION: Enter the overall security classification of the report. Indicate whether "Restricted Data" is included. Marking is to be in accordance with appropriate security regulations.

2b. GROUP: Automatic downgrading is specified in DoD Directive 5200.10 and Armed Forces Industrial Manual. Enter the group number. Also, when applicable, show that optional markings have been used for Group 3 and Group 4 as authorized.

3. REPORT TITLE: Enter the complete report title in all capital letters. Titles in all cases should be unclassified. If a meaningful title cannot be selected without classification, show title classification in all capitals in parenthesis immediately following the title.

4. DESCRIPTIVE NOTES: If appropriate, enter the type of report, e.g., interim, progress, summary, annual, or final. Give the inclusive dates when a specific reporting period is covered.

5. AUTHOR(S): Enter the name(s) of author(s) as shown on or in the report. Enter last name, first name, middle initial. If military, show rank and branch of service. The name of the principal author is an absolute minimum requirement.

6. REPORT DATE: Enter the date of the report as day, month, year, or month, year. If more than one date appears on the report, use date of publication.

7a. TOTAL NUMBER OF PAGES: The total page count should follow normal pagination procedures, i.e., enter the number of pages containing information.

7b. NUMBER OF REFERENCES: Enter the total number of references cited in the report.

8a. CONTRACT OR GRANT NUMBER: If appropriate, enter the applicable number of the contract or grant under which the report was written.

8b, 8c, & 8d. PROJECT NUMBER: Enter the appropriate military department identification, such as project number, subproject number, system numbers, task number, etc.

9a. ORIGINATOR'S REPORT NUMBER(S): Enter the official report number by which the document will be identified and controlled by the originating activity. This number must be unique to this report.

9b. OTHER REPORT NUMBER(S): If the report has been assigned any other report numbers (either by the originator or by the sponsor), also enter this number(s).

10. AVAILABILITY/LIMITATION NOTICES: Enter any limitations on further dissemination of the report, other than those imposed by security classification, using standard statements such as:

(1) "Qualified requesters may obtain copies of this report from DDC."

(2) "Foreign announcement and dissemination of this report by DDC is not authorized."

(3) "U.S. Government agencies may obtain copies of this report directly from DDC. Other qualified DDC users shall request through

_____."

(4) "U.S. military agencies may obtain copies of this report directly from DDC. Other qualified users shall request through

_____."

(5) "All distribution of this report is controlled. Qualified DDC users shall request through

_____."

If the report has been furnished to the Office of Technical Services, Department of Commerce, for sale to the public, indicate this fact and enter the price, if known.

11. SUPPLEMENTARY NOTES: Use for additional explanatory notes.

12. SPONSORING MILITARY ACTIVITY: Enter the name of the departmental project office or laboratory sponsoring (paying for) the research and development. Include address.

13. ABSTRACT: Enter an abstract giving a brief and factual summary of the document indicative of the report, even though it may also appear elsewhere in the body of the technical report. If additional space is required, a continuation sheet shall be attached.

It is highly desirable that the abstract of classified reports be unclassified. Each paragraph of the abstract shall end with an indication of the military security classification of the information in the paragraph, represented as (TS), (S), (C), or (U).

There is no limitation on the length of the abstract. However, the suggested length is from 150 to 225 words.

14. KEY WORDS: Key words are technically meaningful terms or short phrases that characterize a report and may be used as index entries for cataloging the report. Key words must be selected so that no security classification is required. Identifiers, such as equipment model designation, trade name, military project code name, geographic location, may be used as key words but will be followed by an indication of technical context. The assignment of links, rules, and weights is optional.

Unclassified

Security Classification